Turbulent flow over a liquid layer revisited: multi-equation turbulence modelling

Lennon Ó Náraigh, Peter D. M. Spelt and Tamer A. Zaki

Journal of Fluid Mechanics / Volume 683 / September 2011, pp 357 - 394
DOI: 10.1017/jfm.2011.281, Published online: 25 August 2011

J. Fluid Mech. (2011), *vol.* 683, *pp.* 357–394.
doi:10.1017/jfm.2011.281

Turbulent flow over a liquid layer revisited: multi-equation turbulence modelling

Lennon Ó Náraigh[1]†, Peter D. M. Spelt[2,3,4] and Tamer A. Zaki[5]

[1] School of Mathematical Sciences, University College Dublin, Belfield, Dublin 4, Ireland

[2] Department of Chemical Engineering, Imperial College London SW7 2AZ, UK

[3] Département Mécanique, Université Claude Bernard Lyon 1, France

[4] Laboratoire de la Mécanique des Fluides & Acoustique (LMFA), CNRS, Ecully, France

[5] Department of Mechanical Engineering, Imperial College London SW7 2AZ, UK

(Received 25 June 2010; revised 21 January 2011; accepted 29 June 2011; first published online 25 August 2011)

The mechanisms by which turbulent shear flow causes waves on a gas–liquid interface are studied analytically, with a critical assessment of the possible role played by wave-induced Reynolds stresses (WIRSs). First, turbulent flow past a corrugated surface of a small slope is analysed; the surface can either be stationary or support a travelling wave. This problem serves as a useful model because direct numerical simulation (DNS) and experimental data are available to test the analysis, and because this picture is itself a model for the fully coupled two-layer problem. It is demonstrated that the WIRSs play no significant role in shear-driven turbulent flow past a moving wavy wall, and that they alter the structure of the flow only in a quantitative fashion in the pressure-driven case. In the shear-driven case in particular, excellent agreement is obtained with previously reported DNS results. Two closure assumptions are made in our model: the first concerns the wave-induced dissipation of turbulent kinetic energy; the second concerns the importance of rapid distortion. The results of our calculations are sensitive to the assumptions used to close the wave-induced dissipation but are insensitive to the details of the rapid-distortion modelling. Finally, the fully coupled two-layer problem is addressed in the setting of waves of small amplitude, where it is demonstrated that the WIRSs do not play a significant role in the growth of interfacial waves, even at relatively high Reynolds numbers. Again, good agreement is obtained between data from experiments and DNS.

Key words: gas/liquid flow, instability, wave–turbulence interactions

1. Introduction

The study of turbulent flow over liquid layers is of importance in a wide range of fields, including wave generation by wind (e.g. Janssen 2004), and as a route to slug flow and droplet entrainment in stratified and annular flows in oil/gas transport and heat exchangers (Hewitt & Hall-Taylor 1970). Although the linear instability and governing mechanisms in the laminar-flow case are well understood based on

† Email address for correspondence: lennon.onaraigh@ucd.ie

the temporal (Yiantsios & Higgins 1988) and spatio-temporal (Valluri *et al.* 2010) analyses, this is true only to a limited degree in the case of turbulent systems. Various possible mechanisms for instability have been identified (for a review, see Boomkamp & Miesen 1996). Good agreement with oceanographic experimental data has been obtained with the model of Miles (see, for example, Janssen 2004). However, the liquid layer is represented in that model as a moving wavy wall. In fact, several detailed experimental and direct numerical simulation (DNS) studies have been reported on this idealized problem. In this setting, the wave-induced perturbation in the gas flow is not coupled with its counterpart in the liquid. This limitation may be important: in reality, the wave speed should follow from a full analysis and not be imposed. Moreover, since the Miles model is inviscid, it cannot account for the viscosity-contrast mechanism (Yih 1967). This mechanism has been found to be dominant in the instability of thin liquid films sheared by turbulence in two-layer channel flow, and linear stability analyses compare well with experimental data (Miesen & Boersma 1995; Kuru *et al.* 1995; Ó Náraigh *et al.* 2011). Finally, the Miles model does not include wave-induced Reynolds stresses (WIRSs) that can feed back into the wave growth, by mechanisms such as rapid distortion.

We herein develop a comprehensive model, which accounts for the WIRSs in three distinct but overlapping scenarios. First, we study turbulent flow past a solid, undulating wall, and we compare our model with the experiments of Hanratty and coworkers (Thorsness, Morrisroe & Hanratty 1978; Zilker, Cook & Hanratty 1976; Hanratty 1983) (the paper of Thorsness *et al.* 1978 also contains a significant amount of modelling work that is discussed further in § 3.1 below). Next, we study turbulent flow past moving wavy walls, which we compare in detail with DNS data. Finally, we study the fully coupled two-layer problem with infinitesimal wave heights, and allow for the viscosity-contrast mechanism. Our aim is to bring these strands together. We start with a review of the literature pertaining to the generation of interfacial waves by a turbulent flow.

In early works, the Reynolds stress terms that enter into the stability equations were ignored, although the turbulent nature of the gas flow was otherwise taken into account through the prescription of a logarithmic mean profile in the gas (Miles 1957, 1959, 1962; Benjamin 1959). This shortcoming was rectified by several authors. Hanratty and coworkers (Hanratty 1983; Abrams & Hanratty 1985) and van Duin & Janssen (1992) pursued an eddy-viscosity approach. In a series of papers, Belcher and coworkers studied the interfacial stability of a sheared two-fluid interface, specializing to an air–water system for oceanographic applications (Belcher & Hunt 1993; Belcher, Harris & Street 1994; Belcher & Hunt 1998). They focused on describing the structure of the turbulent shear stresses in the problem through the use of scaling arguments and a truncated mixing-length model. This is representative of an approximation of a Reynolds-averaged ensemble of realizations of the turbulent flow for a given phase of a small-slope interfacial wave. Hence, an eddy viscosity was formulated in terms of the typical scale of a turbulent eddy, which depends on the distance between the eddy itself and the air–water interface. Far from the interface, the turbulent eddies are advected quickly over an interfacial undulation, and have insufficient time to equilibrate, and so-called rapid-distortion theory (Townsend 1972, 1980) is needed. This region is modelled in a minimal way by Belcher and coworkers using the Rayleigh equation. Thus, the mixing-length is truncated: it is a simple function of the vertical coordinate close to the interface, and is set to zero far from the interface.

We propose instead to follow the approach of Townsend (1980) and Ierley & Miles (2001): not only do we interpolate between the turbulent domains, which is a common

factor between all of these papers, but we also explicitly model the rapid-distortion region. This approach can be regarded as a 'one-and-a-half-equation model', since the single differential equation for the turbulent kinetic energy (TKE) is supplemented with an algebraic closure for the WIRSs. The algebraic equation is based on the linearized closure model of the Reynolds-averaged equations pioneered by Launder, Reece & Rodi (1975). While the latter model is a multi-equation one, Ierley & Miles (2001) found that the one-and-a-half-equation approach was sufficient. In particular, it compared well with numerical simulations of the complete second-order model for turbulent shear flow over a moving wavy wall (Mastenbroek *et al.* 1996; Meirink & Makin 2000). In order not to be restricted to asymptotic regimes, as is the case in most of the work cited above, the problems studied herein are solved using eigenvalue analysis, and a linear-algebra package. This analysis also enables us to reconstruct the velocity and pressure fields.

In § 2 we first develop a theory for turbulent flow past a small-slope undulation, and past a moving wavy wall. This facilitates a comparison with experiments (Zilker *et al.* 1976; Thorsness *et al.* 1978; Abrams & Hanratty 1985) and DNS (Sullivan, McWilliams & Moeng 2000; Kihara *et al.* 2007). Our theory uses Reynolds-averaged Navier–Stokes (RANS) models of increasing complexity in order to close the WIRSs: a quasi-linear model that ignores the WIRSs completely; an eddy-viscosity model (EVM); a one-equation viscoelastic model (VEM); and a model that accounts for rapid distortion of turbulence in the far field of the wall (rapid-distortion theory (RDT)). Equipped with these insights, we revisit the description of the interaction between small-amplitude waves and turbulent flow over a deep liquid layer at high Reynolds number (§ 5). This extends our previous work on thin films sheared by turbulent gas flow (Ó Náraigh *et al.* 2011). Here, the perturbation in the gas layer due to an interfacial wave is fully coupled with its counterpart in the liquid. Special care is taken to prescribe a detailed base-state velocity profile that enables us also to capture a possible viscosity-contrast instability as well as, for instance, the Miles mechanism. Moreover, our prescription does not contain the logarithmic singularities present in other models (Biberg 2007) when the velocity is evaluated at the upper boundary and the interface. This regularization is accomplished by using a viscosity function that transitions smoothly between the log layer and the viscous near-wall and near-interfacial regions. The method used here has been tested extensively against previous work and experimental data for the corresponding problem of a thin liquid film sheared by a turbulent gas flow in pressure-driven channel flow (Ó Náraigh *et al.* 2011).

2. Turbulent flow past a moving wavy wall: modelling and analysis

We consider turbulent flow past a corrugated surface that supports a travelling wave (figure 1). In the laboratory frame, the upper wall ($z = H$) moves at a speed U_{max} and drives the turbulence. We also use a frame that moves with the wave, wherein the Reynolds-averaged flow variables appear stationary. In this moving frame, the streamwise fluid velocity at the wavy wall takes the value $-c$. The slope of the sinusoidal undulation of the bottom wall is assumed to be infinitesimally small, i.e. $a\alpha \ll 1$. Note, however, that in this section there is no requirement for the wave amplitude a to be infinitesimally small. This framework enables us to compare our results with previously reported simulations and experiments.

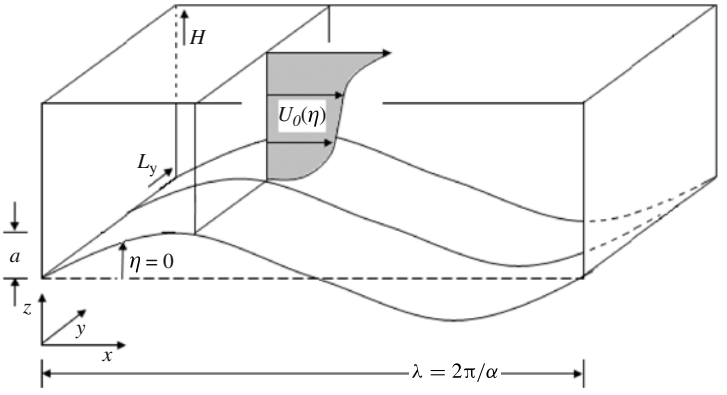

FIGURE 1. Schematic description of flow past a wavy wall.

2.1. *Base-state averaged velocity profile*

We first of all consider the case where the bottom wall is flat and stationary ($a = 0$, $c = 0$). We derive the unidirectional mean velocity $U_0(z)$ from the stationary RANS equations with eddy viscosity $\mu_T(z)$:

$$\left[\frac{1}{Re} + \mu_T(z)\right]\frac{\mathrm{d}U_0}{\mathrm{d}z} = \frac{Re_*^2}{Re^2}, \tag{2.1}$$

where we work in units with $\mu_G = 1$, $\rho_G = 1$, and $H = 1$. The subscript on these parameters denotes a gas phase. This notation becomes useful later in § 5 when we study two-phase gas–liquid flow. The control parameter is the Reynolds number $Re = \rho_G U_{max} H/\mu_G$, of which the friction Reynolds number $Re_* = \rho_G U_* H/\mu_G$ is a function. The eddy viscosity is prescribed in a standard fashion (Biberg 2007; Ó Náraigh & Spelt 2010)

$$\mu_T(z) = \frac{\kappa Re_*}{Re} z(1-z) f(z; C_A) f(1-z; C_A), \tag{2.2}$$

where f is an interpolating function such that the velocity profile and the turbulent shear stress have the correct scaling behaviour as $z \to 0, 1$:

$$f(z; C_A) = 1 - \mathrm{e}^{-(zRe_*)^2/C_A}. \tag{2.3}$$

If we specify $C_A = \mathrm{e}^{5.9}$, ($C_A = \mathrm{e}^{6.3}$ for the corresponding pressure-driven case), then the thickness of the viscous sublayers near the walls is five wall units. Thus, the model velocity is

$$U_0(z) = \frac{Re_*^2}{Re}\int_0^z \frac{\mathrm{d}s}{1 + \kappa Re_* s(1-s) f(s) f(1-s)}, \quad 0 \leqslant z \leqslant 1, \tag{2.4}$$

where the friction velocity Re_* is determined by the upper-plate condition $U_0(1; Re_*) = 1$, i.e.

$$\frac{Re_*^2}{Re}\int_0^1 \frac{\mathrm{d}s}{1 + \kappa Re_* s(1-s) f(s) f(1-s)} = 1. \tag{2.5}$$

Results for a test case are shown in figure 2, together with a comparison with DNS. Figure 2(*a–c*) validates our model: the only parameter that is adjusted is C_A, and that

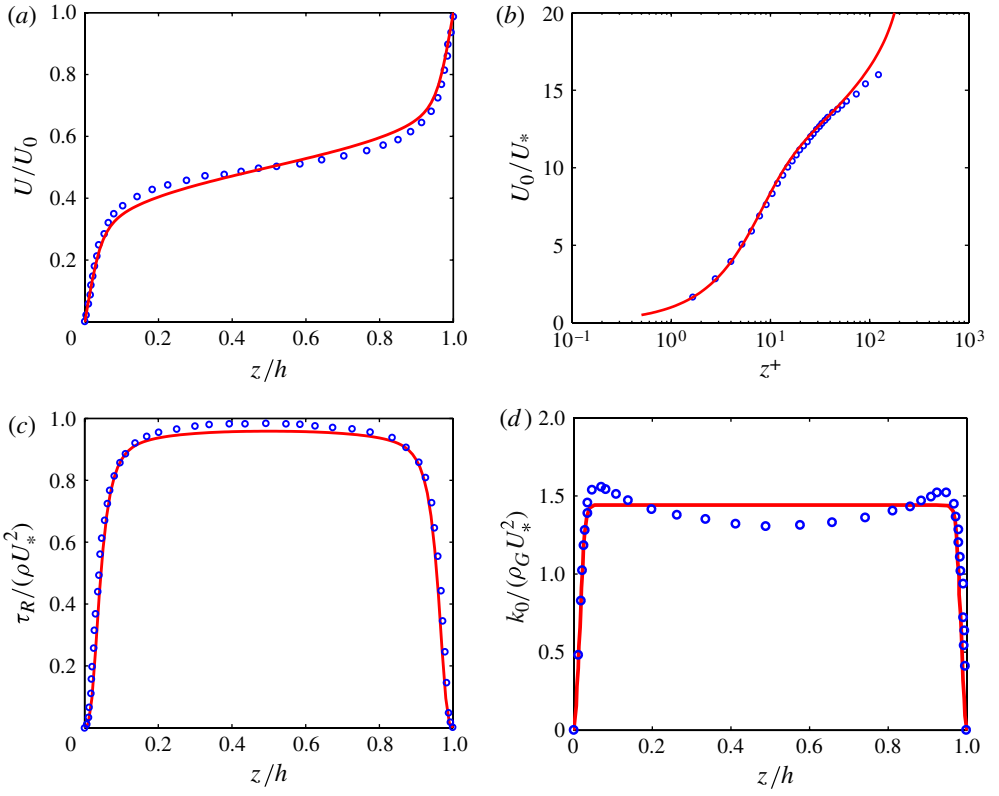

FIGURE 2. Solid lines: model base-state profiles for shear-driven single-phase turbulence (flat bottom, $c = 0$). Dots: the model is validated against the simulations of Sullivan *et al.* (2000) (Figures 6–7 therein). The Reynolds number is $Re = 8000$, based on the upper-plate velocity. (*a*) The base-state velocity profile, across the entire channel width; (*b*) semilog plot of the velocity profile, showing the log layer near the bottom wall; (*c*) the base-state Reynolds-stress profile; (*d*) base-state TKE.

is chosen such that the laminar sublayer is five wall units; this is known *a priori* and is therefore not a fitting parameter.

The balance law for the base-state TKE k_0 is

$$0 = \frac{\mathrm{d}}{\mathrm{d}z}\left[\left(Re^{-1} + \frac{\mu_T}{\sigma_K}\right)\frac{\mathrm{d}k_0}{\mathrm{d}z}\right] + \tau_0(z)\frac{\mathrm{d}U_0}{\mathrm{d}z} - \mathscr{E}_0, \tag{2.6}$$

where σ_K is an empirical prefactor which we henceforth set equal to unity (Pope 2000), $\tau_0 = \mu_T U_0'$, and where $\mathscr{E}_0$ is the dissipation function to be determined. In contrast to the standard treatment, wherein a specification of $\mathscr{E}_0$ fixes k_0, we specify a solution k_0, which then fixes the dissipation $\mathscr{E}_0$. Thus, we approximate k_0 by

$$k_0 = \frac{1}{C_K^2}\frac{Re_*^2}{Re^2} f(z; C_B) f(1 - z; C_B), \tag{2.7}$$

where C_K is an $O(1)$ constant and the slope C_B is chosen such that the kinetic energy is within 1 % of its maximum value at 20 wall units from the wall (Pope 2000). We take $C = 0.83$ for shear-driven flow, to agree with the DNS database of Sullivan *et al.* (2000), and $C = 0.55$ for pressure-driven flow, as in the work of Pope (2000). The

advantage of such an approach is that the TKE has the correct asymptotic behaviour, $k_0 \sim z^2$ as $z \to 0$. Other work (Boomkamp & Miesen 1996) demonstrates that this region has a critical effect on interfacial instability, and such asymptotic behaviour is therefore not ignorable. A comparison between this approximate functional form and DNS for shear-driven single-phase channel flow is shown in figure 2(*d*). Our functional form (2.7) should only be regarded as a 'fit', and the loose agreement between the two descriptions is adequate for our purposes. Having now constituted the turbulent base state, we turn to an analysis of small perturbations around this state, and the wave-turbulence interactions evinced by these perturbations.

2.2. *Flow decomposition*

To understand the averaging method presumed herein, consider a flow domain that comprises periodic copies of the basic domain in figure 1, which extends indefinitely in the x-direction. For definiteness, we work in a frame moving with the wave, although the decomposition carries over into the laboratory frame by a simple Galilean transformation. Periodic boundary conditions are imposed in the y-direction. In Cartesian coordinates, the instantaneous velocity $(u_{cart}, v_{cart}, w_{cart})$ is decomposed into mean and fluctuating parts:

$$\left.\begin{aligned} u_{cart}(x,y,z,t) &= \overline{u_{cart}}(x,z) + u'_{cart}(x,y,z,t), \\ v_{cart}(x,y,z,t) &= v'_{cart}(x,y,z,t), \\ w_{cart}(x,y,z,t) &= \overline{w_{cart}}(x,z) + w'_{cart}(x,y,z,t), \end{aligned}\right\} \tag{2.8}$$

where, for any signal $A(x,y,z,t)$, the Reynolds averages $\overline{A}(x,z)$ and $\langle A\rangle(z)$ are defined as

$$\overline{A}(x,z) = \lim_{T\to\infty}\lim_{N\to\infty}\frac{1}{T}\frac{1}{(2N+1)}\frac{1}{L_y}\sum_{n=-N}^{N}\int_0^T \mathrm{d}t\int_0^{L_y}\mathrm{d}y\, A(x+n\lambda, y, z, t), \tag{2.9}$$

$$\langle A\rangle(z) = \frac{1}{L_x}\int_0^{L_x}\mathrm{d}x\,\overline{A}(x,z). \tag{2.10}$$

In the z-direction, the bottom boundary is located at $z = h_0(x)$ in the moving frame. In boundary-fitted coordinates $\eta = z - a\mathrm{e}^{-\alpha z}\mathrm{e}^{\mathrm{i}\alpha x}$ and $\xi = x - \mathrm{i}a\mathrm{e}^{-\alpha z}\mathrm{e}^{\mathrm{i}\alpha x}$, the bottom boundary is given by $\eta = 0$. Here, the real part of the expressions is assumed implicitly. The total Reynolds-averaged field $\overline{A}(x,z)$ is re-expressed as $\overline{A}(\xi,\eta)$, and is then decomposed further into a part associated with the mean, streamwise flow and a wave-induced variation:

$$\overline{A}(x,z) = A_0(\eta) + \overline{A}(\eta,\xi), \quad A_0(\eta) = \frac{1}{L_\xi}\int \mathrm{d}\xi\,\overline{A}(\eta,\xi), \tag{2.11}$$

where L_ξ is an appropriate scale factor. Further discussion of these coordinates is given in § 2.3. In the present case, where $a\alpha$ is small, it is appropriate to assume that the system responds linearly to the presence of the wavy wall. Thus, (2.11) becomes

$$\overline{A}(x,z) = A_0(\eta) + a\mathrm{e}^{\mathrm{i}\alpha\xi}\hat{A}(\eta). \tag{2.12}$$

Note finally that in the moving frame, the Reynolds average $\overline{A}(x,z)$ appears stationary; however, upon transforming back into the laboratory frame, a wavelike time dependence is introduced, $\overline{A}(x,z) \to \overline{A}(x-ct,z)$. This result is of particular relevance to § 4, where we compute the time change of the kinetic energy in the laboratory frame.

We now apply these averaging concepts to the average velocity profile generated by the wavy wall and the turbulence in figure 1.

2.3. *Undulation-induced perturbations*

In order to determine the wave-induced fields, which are finite, we use boundary-fitted coordinates in the frame of reference moving with the wave. This enables a linear analysis for small-slope waves $a\alpha \ll 1$. Specifically, we use the boundary-layer coordinates advocated by Benjamin (1959) and others (Belcher *et al.* 1994; Tseluiko & Kalliadasis 2011). Note that the coordinates used by Hanratty and coworkers (Zilker *et al.* 1976; Abrams & Hanratty 1985) give similar results. Here, we introduce the transformations

$$\xi = x - \mathrm{i}a\Phi, \quad \eta = z - a\Phi, \quad \Phi = \mathrm{e}^{-\alpha z}\mathrm{e}^{\mathrm{i}\alpha x}. \tag{2.13}$$

By definition, the direction vectors associated with this coordinate system are $\boldsymbol{e}_\xi = \partial \boldsymbol{x}/\partial\xi$ and $\boldsymbol{e}_\eta = \partial \boldsymbol{x}/\partial\eta$. To order αa, these are orthogonal and equal to

$$\boldsymbol{e}_\xi = (1 - a\alpha\Phi, \mathrm{i}a\alpha\Phi), \tag{2.14a}$$

$$\boldsymbol{e}_\eta = (-\mathrm{i}\alpha a\Phi, 1 - a\alpha\Phi), \tag{2.14b}$$

while the lowest-order expansion for the scale factors $h_\xi = |\boldsymbol{e}_\xi|$ and $h_\eta = |\boldsymbol{e}_\eta|$ is given by

$$h := h_\xi = h_\eta = 1 - \alpha a\Phi. \tag{2.15}$$

The disturbance due to the wavy wall is determined in a frame of reference moving with the wave. The total stream function corresponding to the two-dimensional Reynolds-averaged velocity field is written in the following form, according to the decomposition (2.12):

$$\overline{\psi} = \int_0^\eta [U_0(s) - c]\,\mathrm{d}s + a\mathrm{e}^{\mathrm{i}\alpha\xi}\hat{F}(\eta). \tag{2.16}$$

Throughout this paper, we use $U_0(\cdot)$ to denote the non-wave-induced, average streamwise velocity in the laboratory frame. Hence, the Reynolds-averaged velocity components in the directions $\boldsymbol{e}_\xi$ and $\boldsymbol{e}_\eta$ are

$$\overline{u}(\eta, \xi) = h^{-1}\overline{\psi}_\eta = U_0(\eta) - c + a\mathrm{e}^{\mathrm{i}\alpha\xi}[\alpha\mathrm{e}^{-\alpha\eta}(U_0(\eta) - c) + \hat{F}'(\eta)], \tag{2.17a}$$

$$\overline{w}(\eta, \xi) = -h^{-1}\overline{\psi}_\xi = -\mathrm{i}\alpha a\mathrm{e}^{\mathrm{i}\alpha\xi}\hat{F}(\eta). \tag{2.17b}$$

Note, however, that the velocity components in the *Cartesian* directions are the following:

$$\overline{u_{cart}}(\eta, \xi) = \overline{\psi}_z = U_0(\eta) - c + a\mathrm{e}^{\mathrm{i}\alpha\xi}[\alpha\mathrm{e}^{-\alpha\eta}(U_0(\eta) - c) + \hat{F}'(\eta)], \tag{2.18a}$$

$$\overline{w_{cart}}(\eta, \xi) = -\overline{\psi}_x = -\mathrm{i}\alpha a\mathrm{e}^{\mathrm{i}\alpha\xi}[\hat{F}(\eta) - (U_0(\eta) - c)]. \tag{2.18b}$$

To make the correspondence between these results and the averaging concept in § 2.2 explicit, we re-write these equations as

$$\overline{u_{cart}}(\eta, \xi) = U_0(\eta) - c + \tilde{u}(\eta, \xi), \tag{2.19a}$$

$$\overline{w_{cart}}(\eta, \xi) = \tilde{w}(\eta, \xi). \tag{2.19b}$$

By applying this formalism, we write down an equation for momentum balance, expressed in the stream function ψ, and the curvilinear coordinates (2.13):

$$-\frac{1}{h_\xi h_\eta}\left[\frac{\partial\overline{\psi}}{\partial\xi}\frac{\partial}{\partial\eta}\Delta\overline{\psi}-\frac{\partial\overline{\psi}}{\partial\eta}\frac{\partial}{\partial\xi}\Delta\overline{\psi}\right]=\frac{1}{Re}\Delta^2\overline{\psi}+\text{Reynolds-stress contributions.} \quad (2.20)$$

Later on, we use this equation to write down an explicit equation for $\hat{F}(\eta)$. Before doing so, we determine the boundary conditions on $\hat{F}(\eta)$, and characterize the Reynolds-stress contributions in (2.20).

2.4. *Boundary conditions*

The boundary conditions at the top wall $z=1$ are linearized onto the surface $\eta=1$, with an error that is $O(a\mathrm{e}^{-\alpha})$. Thus, $\hat{F}=\hat{F}'=0$ there. At $\eta=0$, the $\hat{F}$ boundary conditions take either of the following forms, according to the nature of the wavy wall. We work in a frame moving with the wave.

(a) Stationary wavy wall:

$$\overline{u_{cart}}=0, \quad \overline{w_{cart}}=0, \text{ hence } \hat{F}'(0)=0, \hat{F}(0)=0. \quad (2.21)$$

(b) The bottom mimics an Airy wave (Acheson 1990):

$$\overline{u_{cart}}=-c+\alpha ac\mathrm{e}^{\mathrm{i}\alpha x}, \quad \overline{w_{cart}}=-\mathrm{i}\alpha ac\mathrm{e}^{i\alpha x}, \text{ hence } \hat{F}'(0)=2\alpha c, \hat{F}(0)=0. \quad (2.22)$$

Condition (b) corresponds to $\beta=-\alpha c$ in the discussion by Benjamin (1959); to lowest order, it satisfies the free-surface condition

$$\overline{w_{cart}}=\overline{u_{cart}}\frac{\partial h_0}{\partial x}, \quad (2.23)$$

where $z=h_0(x)$ is the location of the wavy wall. The wall shear stress is equal to the off-diagonal term in the viscous stress tensor $\overline{T}_{ij}$ (Benjamin 1959), and is therefore given by

$$\begin{aligned}\overline{T}_{xz}(\eta=0)&=Re^{-1}(\overline{\psi}_{zz}-\overline{\psi}_{xx})_{\eta=0},\\&=Re^{-1}U_0'(0)Re^{-1}a\mathrm{e}^{\mathrm{i}\alpha\xi}\\&\quad\times[(\partial_\eta^2+\alpha^2)\hat{F}(\eta)+2\alpha U_0'(\eta)\mathrm{e}^{-\alpha\eta}-2\alpha^2(U_0(\eta)-c)\mathrm{e}^{-\alpha\eta}]_{\eta=0},\\&=Re^{-1}U_0'(0)+\widetilde{T_{xz}}(\eta=0). \quad (2.24)\end{aligned}$$

To obtain appropriate boundary conditions on the turbulence intensity, we recall the decomposition (2.8) of the instantaneous Cartesian velocities into mean and fluctuating components. Near the wall $\eta=0$, the following Taylor expansions hold:

$$u'\sim a_1+a_2\eta+a_3\eta^2+\cdots, \quad (2.25a)$$
$$v'\sim b_1+b_2\eta+b_3\eta^2+\cdots, \quad (2.25b)$$
$$w'\sim c_1+c_2\eta+c_3\eta^2+\cdots. \quad (2.25c)$$

The flow assumes its mean value on the walls, hence $u'=v'=w'=0$ on $\eta=0$, and $a_1=b_1=c_1=0$. Since (η,ξ,y) are independent coordinates, it also follows that

$$\frac{\partial u'}{\partial\xi}=\frac{\partial v'}{\partial\xi}=\frac{\partial w'}{\partial\xi}=0 \quad \text{on } \eta=0, \quad (2.26)$$

and that

$$\frac{\partial u'}{\partial y} = \frac{\partial v'}{\partial y} = \frac{\partial w'}{\partial y} = 0 \quad \text{on } \eta = 0. \tag{2.27}$$

Hence, the continuity equation for the turbulent fluctuations, $u'_x + v'_y + w'_z = 0$, reduces to

$$\frac{\partial u'}{\partial \eta}\frac{\partial \eta}{\partial x} + \frac{\partial w'}{\partial \eta}\frac{\partial \eta}{\partial z} = 0 \quad \text{on } \eta = 0. \tag{2.28}$$

In other words,

$$-\mathrm{i}\alpha a\Phi\frac{\partial u'}{\partial \eta} + \frac{\partial w'}{\partial \eta}(1 + a\alpha\Phi) = 0 \quad \text{on } \eta = 0. \tag{2.29}$$

Hence,

$$c_2 = \mathrm{i}a_2 a\alpha\Phi. \tag{2.30}$$

Using this information, we deduce that the intensity vanishes quadratically as $\eta \to 0$:

$$\tfrac{1}{2}\overline{u'^2 + v'^2 + w'^2} \sim \tfrac{1}{2}\overline{a_2^2 + b_2^2}\eta^2 := \tfrac{1}{2}(A_0 + a\mathrm{e}^{\mathrm{i}\alpha\xi}A_1)\eta^2, \quad \eta \to 0. \tag{2.31}$$

This can be re-written as

$$\tilde{k}(\eta, \xi) \sim \tfrac{1}{2}a\mathrm{e}^{\mathrm{i}\alpha\xi}A_1\eta^2, \quad \eta \to 0. \tag{2.32}$$

In a similar manner, we deduce that the Reynolds stress vanishes quadratically:

$$-\overline{u'w'} \sim -\overline{a_1 b_1}\eta^2 = -\mathrm{i}a\alpha\Phi\overline{a_2^2}\eta^2, \quad \eta \to 0, \tag{2.33}$$

or

$$-\overline{u'w'} \sim -\mathrm{i}a\alpha\Phi k_0(\eta), \quad \eta \to 0. \tag{2.34}$$

We decompose $-\overline{u'w'}$ into a mean part and a wave-induced part: $-\overline{u'w'} = \tau_0(\eta) + \tilde{\tau}(\eta, \xi)$. Since $\tau_0(\eta) \sim \eta^3$ as $\eta \to 0$, it follows that

$$\tilde{\tau}(\eta, \xi) \propto -\mathrm{i}a\alpha\Phi k_0(\eta), \quad \eta \to 0. \tag{2.35}$$

Thus, the appropriate boundary condition on $\tilde{\tau}(\eta = 0)$ is the vanishing one, with an imposed phase shift of $\pi/2$ relative to the wavy wall. Finally, and in the same manner, the dissipation

$$\mathscr{E} = \frac{1}{Re}\overline{s'_{ij}s'_{ij}}, \quad s'_{ij} = \frac{1}{2}\left(\frac{\partial u'_i}{\partial x_j} + \frac{\partial u'_j}{\partial x_i}\right) \tag{2.36}$$

decomposes into mean and wave-induced parts, near $\eta = 0$:

$$\mathscr{E}_0(\eta) + \tilde{\mathscr{E}}(\eta, \xi) \sim \frac{1}{Re}k_0''(\eta) + \frac{1}{Re}[\partial_\eta^2\tilde{k} + 2a\alpha k_0''(\eta)\mathrm{e}^{-\alpha z}] \quad \text{as } \eta \to 0. \tag{2.37}$$

We now turn to the modelling of the turbulent stresses and intensity in the bulk flow.

2.5. *Reynolds-stress contributions*

We continue to work in a frame moving with the wave. Several models for the Reynolds stress tensor $\mathscr{R}_{ij}$ are appended to the vorticity (2.20) in the following coordinate-free manner:

$$\text{Reynolds-stress contributions} = -\hat{\boldsymbol{y}} \cdot [\mathrm{curl}(\mathrm{div}\,\mathscr{R})], \tag{2.38}$$

where $\hat{\boldsymbol{y}}$ is the unit vector perpendicular to the (x, z) plane. In order of complexity, these models are: a quasi-laminar (QL) model wherein turbulence is only accounted for in the specification of the base-state profile; an EVM; a viscoelastic description which uses a one-equation turbulence model; and a rapid-distortion model. We summarize these below, and omit details that rely on standard results (a separate document, describing in detail these calculations, and those of the energy budget in § 4, is available upon request from the corresponding author).

2.5.1. *The QL model*

The QL formalism was first used by Miles (1957). In this approach, the effects of the turbulence appear only through the base state, and the WIRSs are simply set to zero. Miles (1957) ignored molecular viscosity. Here, however, it is included. Thus, we solve the stream function equation in curvilinear coordinates, linearized to include only the fundamental mode:

$$\begin{aligned} &\mathrm{i}\alpha[(U_0(\eta) - c)(\partial_\eta^2 - \alpha^2)\hat{F}(\eta) - U_0''(\eta)(\eta)\hat{F}(\eta)] + \mathscr{C} \\ &\quad = \frac{1}{Re}(\partial_\eta^2 - \alpha^2)^2\hat{F}(\eta), \end{aligned} \tag{2.39}$$

where $\mathscr{C}$ is the curvature-related term

$$\mathscr{C} = 2\mathrm{i}\alpha^2 U_0'(\eta)(U_0(\eta) - c)\mathrm{e}^{-\alpha\eta} + \frac{1}{Re}\mathrm{e}^{-\alpha\eta}[4\alpha^2 U_0''(\eta) - 2\alpha U_0'''(\eta)]. \tag{2.40}$$

2.5.2. *The EVM*

In this model, there is still only a single equation to solve, namely the momentum equation, and the WIRSs are modelled as being proportional to the rate of strain, the constant of proportionality being the base-state eddy viscosity. Thus,

$$\begin{aligned} &\mathrm{i}\alpha[(U_0(\eta) - c)(\partial_\eta^2 - \alpha^2)\hat{F}(\eta) - U_0''(\eta)\hat{F}(\eta)] + \mathscr{C} \\ &\quad = \frac{1}{Re}(\partial_\eta^2 - \alpha^2)^2\hat{F}(\eta) + \mathscr{R}, \end{aligned} \tag{2.41}$$

where $\mathscr{C}$ is the curvature term, and $\mathscr{R}$ is the Reynolds-stress term:

$$\begin{aligned} \mathscr{R} = (\partial_\eta^2 + \alpha^2)\{\mu_T(\eta)[(\partial_\eta^2 + \alpha^2)\hat{F}(\eta) + 2\mathrm{e}^{-\alpha\eta}(\alpha U_0'(\eta) - \alpha^2(U_0(\eta) - c))]\} \\ + 2\mathrm{e}^{-\alpha\eta}[\alpha\tau_0''(\eta) - \alpha^2\tau_0'(\eta)], \quad \tau_0 = \mu_T U_0'. \end{aligned} \tag{2.42}$$

2.5.3. *The viscoelastic model*

The following formulation is similar to that given by Ierley & Miles (2001). We base the description of the Reynolds stresses on the Cartesian anisotropy tensor

$$\boldsymbol{n}_{ij} = \frac{\overline{u_i' u_j'}}{\sum_\ell \overline{u_\ell' u_\ell'}} = -\frac{\mathscr{R}_{ij}}{2k} = -\frac{1}{2k}\begin{pmatrix} \sigma_x & \tau \\ \tau & \sigma_z \end{pmatrix}. \tag{2.43}$$

The turbulence is assumed to tend quickly to equilibrium, and the $\boldsymbol{n}_{ij}$ take their constant value (Ierley & Miles 2001). Thus,

$$\widetilde{\boldsymbol{n}_{12}} = 0, \tag{2.44}$$

hence $\widetilde{-\tau/k} = 0$, and

$$\tilde{\tau} = \frac{\tau_0}{k_0}\tilde{k} = \frac{\tau_0}{k_0} a\mathrm{e}^{\mathrm{i}\alpha\xi}\hat{Q}(\eta). \tag{2.45}$$

Here $\hat{Q}(\eta)$ is the wave-induced component of the TKE. As in standard treatments of shear turbulence (Belcher & Hunt 1998; Pope 2000), we focus only on the off-diagonal stress terms, and assume equipartition of turbulent energy throughout the flow, hence $\widetilde{\boldsymbol{n}_{11}} - \widetilde{\boldsymbol{n}_{22}} = 0$. Thus, the Reynolds-stress contribution in the vorticity (2.20) becomes

$$\mathscr{R} = (\partial_\eta^2 + \alpha^2)\left(\frac{\tau_0}{k_0}\hat{Q}\right) + 2\mathrm{e}^{-\alpha\eta}\left(\alpha\frac{\mathrm{d}^2\tau_0}{\mathrm{d}\eta^2} - \alpha^2\frac{\mathrm{d}\tau_0}{\mathrm{d}\eta}\right). \tag{2.46}$$

Next, we formulate an equation for the wave-induced TKE. The governing equation for $k_0 + \tilde{k}$ can be written in coordinate-free form as

$$(\partial_t + \overline{\boldsymbol{u}} \cdot \boldsymbol{\nabla})(k_0 + \tilde{k}) = \mathrm{div}[(Re^{-1} + \mu_T(\eta))\mathrm{grad}(k_0 + \tilde{k})] + \mathscr{P} - \mathscr{E}. \tag{2.47}$$

Here the left-hand side represents the advection of the energy, and the first term on the right-hand side is the energy flux. In Townsend (1972, 1980) and Ierley & Miles (2001), the energy flux was ignored, since turbulent transport is negligible in the bulk gas flow. It is important, however, near the wavy wall, where molecular viscosity dominates; that is why it is included here. The production function $\mathscr{P}$ is available in closed form through the contraction of two Cartesian tensors:

$$\mathscr{P} = \mathscr{R}_{ij}\frac{\partial \overline{u}_i}{\partial x_j}. \tag{2.48}$$

Next, we decompose the dissipation into equilibrium and wave-induced parts:

$$\mathscr{E} = \mathscr{E}_0(\eta) + \tilde{\mathscr{E}} = \mathscr{E}_0(\eta) + a\mathrm{e}^{\mathrm{i}\alpha\xi}\hat{\mathscr{E}}(\eta). \tag{2.49}$$

For the wave-induced part, we assume that the dissipation of TKE depends on the energy itself. In other words, we assume that $\tilde{\mathscr{E}} \propto \tilde{k}$, with a constant of proportionality that is given by the inverse of the large-eddy time scale. Dimensional analysis suggests that we take this inverse time scale to be $C_D U_0'$, where C_D is an $O(1)$ constant, selected such that the production never exceeds the dissipation (Pope 2000), $C_D = \max(\tau_0/k_0)$:

$$\hat{\mathscr{E}}(\eta) = C_D U_0' \hat{Q} + \text{Boundary terms}. \tag{2.50}$$

This prescription is equivalent to a mixing-length formalism: the mixing length ℓ_0 associated with the dissipation function (2.50) is given by $k_0^{1/2}/\ell_0 = C_D U_0'$. Recasting the closure hypothesis in this way highlights the similarities between our approach and that of other authors (Ierley & Miles 2001; Townsend 1972, 1980). The boundary terms relate to the value assumed by the wave-induced dissipation at the boundary (2.37). Thus, we estimate $\partial_\eta^2\hat{Q}(0)$ as $\alpha k_0''(0)$, and, with reference to (2.37), we take

$$\hat{\mathscr{E}}(\eta) = C_D U_0'\hat{Q} + Re^{-1}[1 - f(z; C_B)]3\alpha k_0''(0). \tag{2.51}$$

Combining these facts, we obtain the following kinetic-energy equation in curvilinear coordinates:

$$
\begin{aligned}
&\mathrm{i}\alpha[(U_0(\eta)-c)\hat{Q}(\eta)-\hat{F}(\eta)k_0'(\eta)]\\
&\quad=[Re^{-1}+\mu_T(\eta)](\partial_\eta^2-\alpha^2)\hat{Q}(\eta)+\mu_T'(\eta)\hat{Q}'(\eta)\\
&\qquad+2\alpha\mathrm{e}^{-\alpha\eta}\{[Re^{-1}+\mu_T(\eta)]k_0''(\eta)+\mu_T'(\eta)k_0'(\eta)\}+\frac{\tau_0(\eta)U_0'(\eta)\hat{Q}(\eta)}{k_0(\eta)}\\
&\qquad+\tau_0(\eta)\{(\partial_\eta^2+\alpha^2)\hat{F}(\eta)+2\mathrm{e}^{-\alpha\eta}[\alpha U_0'(\eta)-\alpha^2(U_0(\eta)-c)]\}\\
&\qquad-C_D U_0'\hat{Q}-Re^{-1}[1-f(z;C_B)]3\alpha k_0''(0).
\end{aligned}
\tag{2.52}
$$

2.5.4. *The complete rapid-distortion model*

Rapid distortion exists as a limiting case wherein the transport equation for the Reynolds stresses becomes linear as a consequence of strong mean strain. This regime of turbulence has been implicated in the formation of waves in turbulent stratified flow (Belcher & Hunt 1993; Belcher *et al.* 1994; Belcher & Hunt 1998). By dividing the turbulence layer into distinct domains (Belcher & Hunt 1998; Cohen & Belcher 1998), our model can be modified to take account of this effect.

The turbulence is characterized by two time scales: the eddy turnover time scale and the advection time scale. The eddy turnover or turbulent time scale is the time required for a typical turbulent eddy to interact with the surrounding fluid and come into equilibrium. An estimate of this time scale, at a distance z from the wavy wall, is $T_t(z)=(\mathrm{d}U_0/\mathrm{d}z)^{-1}$. The advection time scale is the time needed for the flow to advect an eddy over a wave crest. This flow distorts the turbulence and moves it away from equilibrium. An estimate of this time scale is $T_a=[\alpha|U_0(z)-c|]^{-1}$, where α is the wavenumber and c is the (possibly complex) wave speed. Near the wavy wall, T_t is small compared with T_a: this is the region of near-equilibrium where by definition eddy viscosity and one-equation turbulent closures are expected to be appropriate. Far away from the wavy wall, T_t is large compared with the advection time scale (at least for the large, most energetic turbulent structures): this is the region where rapid-distortion theory is expected to apply. Crossover of domains occurs at $z=z_t$, for which $T_t(z_t)=T_a(z_t)$.

In the rapid-distortion domain, and in Cartesian coordinates, the Reynolds-stress equation is

$$
\frac{\partial}{\partial t}(-\mathscr{R}_{ij})+\frac{\partial}{\partial x_k}[\overline{u}_k(-\mathscr{R}_{ij})+\mathscr{T}_{kij}]=\mathscr{P}_{ij}+\mathscr{S}_{ij}^{(r)},
\tag{2.53}
$$

where $\mathscr{T}_{kij}$ and $\mathscr{P}_{ij}$ represent transport and production, respectively, and where $\mathscr{S}_{ij}^{(r)}$ represents the correlation between the rapid pressure, and the rate of strain (Pope 2000). For waves, the shear rate $\alpha(U_0-c)$ enters into the advection term in (2.53). In the rapid-distortion domain, this rate is large, and thus advective transport dominates over pressure-driven transport. We therefore omit the pressure transport term in (2.53), which now simplifies further:

$$
\left(\frac{\partial}{\partial t}+\overline{\boldsymbol{u}}\cdot\boldsymbol{\nabla}\right)(-\mathscr{R}_{ij})=\mathscr{P}_{ij}+\mathscr{S}_{ij}^{(r)}.
\tag{2.54}
$$

The rapid pressure rate of strain tensor $\mathscr{S}_{ij}^{(r)}$ has been modelled accurately by Launder *et al.* (1975) (see also Pope 2000). They use the following form:

$$
\mathscr{S}_{ij}^{(r)}=-C_R(\mathscr{P}_{ij}-\tfrac{1}{2}\mathscr{P}_{kk}\delta_{ij}),
\tag{2.55}
$$

where C_R is a constant that can be determined from DNS databases (we use $C_R = 0.6$, as suggested by Pope 2000). This description has the property of linearity in $\mathscr{R}_{ij}$, which is desirable in any rapid-distortion theory (Pope 2000). Linearizing (2.54) and (2.55) around a base state $(\boldsymbol{n}_{11}^{(0)}, \boldsymbol{n}_{22}^{(0)}, \boldsymbol{n}_{12}^{(0)})$ gives the following balance law for $\widetilde{\boldsymbol{n}_{12}}$ in Cartesian coordinates:

$$\begin{aligned}\left(\frac{\partial}{\partial t} + \overline{\boldsymbol{u}} \cdot \boldsymbol{\nabla}\right) \widetilde{\boldsymbol{n}_{12}} &= [2(\boldsymbol{n}_{12}^{(0)})^2 - (1 - C_R)\boldsymbol{n}_{11}^{(0)}] \frac{\partial}{\partial x} \widetilde{u_{cart}} \\ &\quad + [2(\boldsymbol{n}_{12}^{(0)})^2 - (1 - C_R)\boldsymbol{n}_{22}^{(0)}] \frac{\partial}{\partial z} \widetilde{u_{cart}} \\ &\quad + 2\boldsymbol{n}_{12}^{(0)}(\boldsymbol{n}_{11}^{(0)} - \boldsymbol{n}_{22}^{(0)}) \frac{\partial}{\partial x} \widetilde{w_{cart}}. \end{aligned} \tag{2.56}$$

In curvilinear coordinates, this becomes

$$\begin{aligned}&\mathrm{i}\alpha \left\{ (U_0 - c)\widetilde{\boldsymbol{n}_{12}} - \mathrm{e}^{\mathrm{i}\alpha\xi} \hat{F}(\eta) \frac{\mathrm{d}\boldsymbol{n}_{12}^{(0)}}{\mathrm{d}\eta} \right\} \\ &\quad = \mathrm{e}^{\mathrm{i}\alpha\xi} [\alpha_1 \mathrm{i}\alpha \hat{F}'(\eta) + \alpha_2 \hat{F}''(\eta) + \alpha_3 \alpha^2 \hat{F}(\eta)] \\ &\qquad + \mathrm{e}^{\mathrm{i}\alpha\xi} \{ \mathrm{e}^{-\alpha\eta} [\mathrm{i}\alpha\alpha_1 (\alpha(U_0 - c) - U_0'(\eta)) \\ &\qquad + \alpha_2 (2\alpha U_0'(\eta) - \alpha^2 (U_0 - c)) - \alpha_3 \alpha^2 (U_0 - c)]\}, \end{aligned} \tag{2.57}$$

where

$$\left.\begin{aligned} \alpha_1 &= 2(\boldsymbol{n}_{12}^{(0)})^2 - (1 - C_R)\boldsymbol{n}_{11}^{(0)}, \\ \alpha_2 &= 2(\boldsymbol{n}_{12}^{(0)})^2 - (1 - C_R)\boldsymbol{n}_{22}^{(0)}, \\ \alpha_3 &= 2\boldsymbol{n}_{12}^{(0)}(\boldsymbol{n}_{11}^{(0)} - \boldsymbol{n}_{22}^{(0)}) = 0. \end{aligned}\right\} \tag{2.58}$$

Next, we identify

$$\tilde{\tau} = a\mathrm{e}^{\mathrm{i}\alpha\xi} \hat{\tau}(\eta), \tag{2.59}$$

and interpolate between the algebraic stress model (2.56) in the far field and the equilibrium description $\widetilde{\boldsymbol{n}_{12}} = 0$ (2.45) in the near field. Thus, we introduce the following hybrid stress model involving an interpolation function $\mathscr{I}(\eta)$:

$$\begin{aligned}&\mathrm{i}\alpha(U_0 - c) \left(-\frac{\hat{\tau}(\eta)}{2k_0} + \frac{\tau_0}{2k_0^2} \hat{Q}(\eta) \right) \mathscr{I}(\eta) + [1 - \mathscr{I}(\eta)] \left(-\frac{\hat{\tau}(\eta)}{2k_0} + \frac{\tau_0}{2k_0^2} \hat{Q}(\eta) \right) \\ &\quad = \mathscr{I}(\eta) \left[\mathrm{i}\alpha \hat{F}(\eta) \frac{\mathrm{d}\boldsymbol{n}_{12}^{(0)}}{\mathrm{d}\eta} + \alpha_1 \mathrm{i}\alpha \hat{F}'(\eta) + \alpha_2 \hat{F}''(\eta) - \alpha_3 \alpha^2 \hat{F}(\eta) \right] \\ &\qquad + \mathrm{e}^{-\alpha\eta} \mathscr{I}(\eta) [\mathrm{i}\alpha\alpha_1 (\alpha(U_0 - c) - U_0'(\eta)) + \alpha_2 (2\alpha U_0'(\eta) - \alpha^2 (U_0 - c)) \\ &\qquad + \alpha_3 \alpha^2 (U_0 - c)], \end{aligned} \tag{2.60}$$

where $\mathscr{I}(\eta)$ is an interpolating function that is zero at $\eta = 0$ and asymptotes to $\mathscr{I} = 1$, with a characteristic length scale z_t. We take

$$\mathscr{I}(s) = 1 - \mathrm{e}^{-(s/z_t)^2} \tag{2.61}$$

because this respects the near-wall condition that $\tilde{\tau}$ and its derivative should vanish at $\eta = 0$. Further manipulation yields an equation for $\hat{\tau}$:

$$\begin{aligned}\hat{\tau}(\eta) = k(\eta)\frac{\tau_0}{k_0} - \mathscr{A}(\eta)\left[\mathrm{i}\alpha\hat{F}(\eta)\frac{\mathrm{d}\boldsymbol{n}_{12}^{(0)}}{\mathrm{d}\eta} + \alpha_1\mathrm{i}\alpha\hat{F}'(\eta) + \alpha_2\hat{F}''(\eta) + \alpha_3\alpha^2\hat{F}(\eta)\right] \\ - \mathrm{e}^{-\alpha\eta}\mathscr{A}(\eta)[\mathrm{i}\alpha\alpha_1(\alpha(U_0 - c) - U_0'(\eta)) + \alpha_2(2\alpha U_0'(\eta) - \alpha^2(U_0 - c)) \\ - \alpha_3\alpha^2(U_0 - c)],\end{aligned} \tag{2.62}$$

where

$$\mathscr{A}(\eta) = \frac{2k_0(\eta)\mathscr{I}(\eta)}{\mathscr{I}(\eta)[\mathrm{i}\alpha(U_0 - c) - 1] + 1}. \tag{2.63}$$

The term

$$\mathrm{i}\alpha\hat{F}(\eta)\frac{\mathrm{d}\boldsymbol{n}_{12}^{(0)}}{\mathrm{d}\eta} \tag{2.64}$$

vanishes in the far field; thus, we take the stress equation to be

$$\begin{aligned}\hat{\tau}(\eta) = \hat{Q}(\eta)\frac{\tau_0}{k_0} - \mathscr{A}(\eta)[\alpha_1\mathrm{i}\alpha\hat{F}'(\eta) + \alpha_2\hat{F}''(\eta) + \alpha_3\alpha^2\hat{F}(\eta)] \\ - \mathrm{e}^{-\alpha\eta}\mathscr{A}(\eta)[\mathrm{i}\alpha\alpha_1(\alpha(U_0 - c) - U_0'(\eta)) + \alpha_2(2\alpha U_0'(\eta) - \alpha^2(U_0 - c)) \\ - \alpha_3\alpha^2(U_0 - c)].\end{aligned} \tag{2.65}$$

We supplement this algebraic equation with the previously developed transport equations for $\hat{Q}$ and $\hat{F}$. Now, however, the Reynolds-stress term $\mathscr{R}$ in the momentum equation is given by

$$\mathscr{R} = (\partial_\eta^2 + \alpha^2)\hat{\tau} + 2\mathrm{e}^{-\alpha\eta}\left(\alpha\frac{\mathrm{d}^2\tau_0}{\mathrm{d}\eta^2} - \alpha^2\frac{\mathrm{d}\tau_0}{\mathrm{d}\eta}\right). \tag{2.66}$$

We call the first three models *stationary* models because the Reynolds stresses are constituted in terms of mean quantities, that is, they are computed diagnostically. In the last case the Reynolds stresses are transported and strained, and are therefore computed as prognostic variables.

Having derived our turbulence model, we proceed to validate it against a database of experiments conducted for flow past a wavy wall.

3. Pressure-driven channel flows: comparison with experiments and simulations

In this section, we compare our theoretical models with the experimental results of Hanratty and coworkers (Zilker *et al.* 1976; Thorsness *et al.* 1978; Abrams & Hanratty 1985) for stationary walls ($c = 0$). These experimental papers form a rigorous challenge for the models of § 2, since they involve a wide range of Reynolds numbers. We also compare our modelling efforts with the DNS paper of Kihara *et al.* (2007). Throughout this section, the base flow is driven by a constant pressure drop in the streamwise direction; we modify the base-state model in § 2 accordingly.

3.1. *Comparisons with experiments*

The computation in the QL EVM cases is straightforward and follows from § 2. For the other models, we take

$$\boldsymbol{n}_{12}^{(0)} = \left.\frac{\tau_0}{2k_0}\right|_{z=1/2} \approx \frac{1}{2}C^2, \tag{3.1}$$

together with $\boldsymbol{n}_{11}^{(0)} = \boldsymbol{n}_{22}^{(0)} = 1/2$ (varying these parameters has little effect on the results of this section). To close the model, we use the mixing-length theory for the wave-induced dissipation (2.50) and (2.51). A more detailed closure model that describes the effects of the wavy wall on the choice of mixing length ℓ can be found in the papers of Hanratty and coworkers ('Model D', Thorsness *et al.* 1978). Although such an approach gives very close agreement with the experimental results, this is not adopted here for a number of reasons. First, Model D involves a 'relaxation' of the wave-induced mixing length to its equilibrium value, a process whose physical mechanism is unclear. Second, Model D involves a fitting parameter, which must be chosen *a posteriori*. The value of this fitting parameter might change as we pass over to shear-driven single-phase flow, or to two-phase flow, and the model is therefore of limited applicability to the present paper. For these reasons, we maintain with the theoretical modelling described in § 2. This approach produces reasonable agreement with the experimental predictions, as we now demonstrate.

We compare the zero-equation models with the experiments of Abrams & Hanratty (1985), wherein the phaseshift between the wave-induced shear stress, and the wavy wall is calculated, as a function of friction Reynolds number, for a given wavy wall $\alpha H = 2\pi$ (figure 3*a*). For small friction Reynolds numbers, the models shown in the comparison curve agree with one another, suggesting that at small Reynolds numbers, the QL approach is valid. Note also that our QL model and that of Abrams & Hanratty (1985) agree closely; any minor differences are due to differences between the coordinate systems. We have favoured the Benjamin coordinates for their simplicity, and because other authors have shown them to be valid in comparisons with experiments (Tseluiko & Kalliadasis 2011). At higher Reynolds numbers, however, the experimental curve exhibits a large local maximum in the phaseshift, which none of the zero-equation models predicts very well. We therefore turn to the viscoelastic description. We apply the mixing-length theory (2.50) and (2.51) for the wave-induced dissipation and obtain the associated phaseshift curve (figure 3*b*). This curve reproduces the sharp maximum in the phaseshift seen in the experiments. Furthermore, in figure 4, we plot the magnitude of the wall shear stress as a function of the friction Reynolds number. The viscoelastic model again gives a good qualitative description of the dependence. Although our results are superior to those produced by the *ab initio* theories developed by Hanratty and co-workers, the lack of precise quantitative agreement is to some degree disappointing. Thus, we systematically review the causes of this lack of agreement.

First, we investigate whether the inclusion of rapid distortion in the description of the turbulence improves the accuracy of the model with respect to the experimental data. We determine the length scale in the interpolation function $\mathscr{I}(\eta) = 1 - \mathrm{e}^{-(\eta/z_t)^2}$ as the boundary between two domains, which is determined by equating a time scale for advection of a turbulent eddy past one wavelength with an eddy decay time, i.e. by the root-finding equation

$$U_0'(z_t) = \alpha U_0(z_t). \tag{3.2}$$

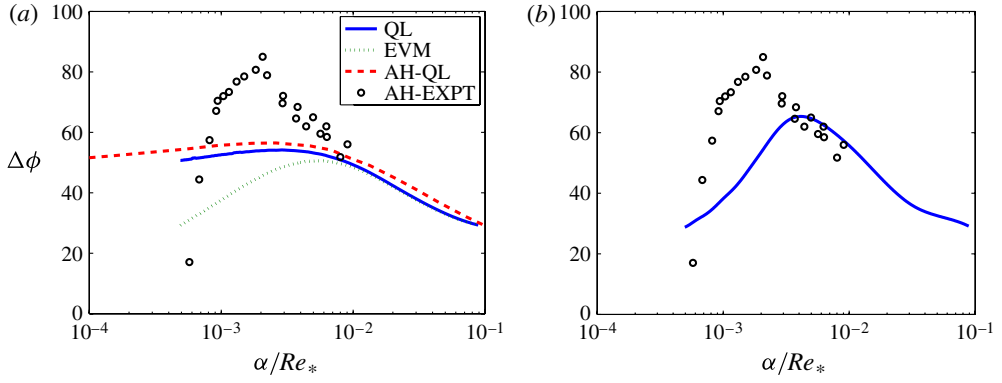

FIGURE 3. Comparison of the phaseshift (in degrees) between the models and the experiment of Abrams & Hanratty (1985). (*a*) Zero-equation models; (*b*) the viscoelastic model, with the wave-induced dissipation determined by the mixing-length theory (2.50) and (2.51).

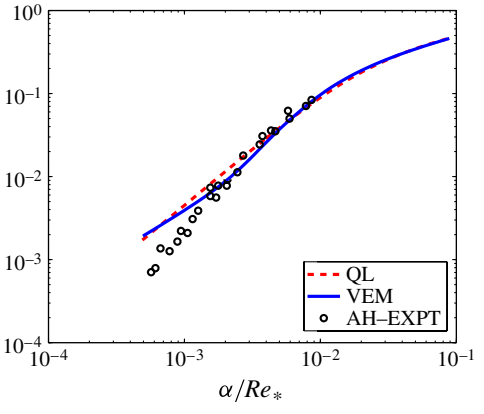

FIGURE 4. The magnitude of the wave-induced interfacial shear stress $(2H|\widehat{T_{xz}}|/\rho_G U_0^2)/Re_*$, as a function of the friction Reynolds number.

The phaseshift study in figure 5 suggests that the inclusion of the rapid distortion does not improve the model predictions. Moreover, the rapid-distortion stream function possesses oscillations that propagate throughout the flow domain (figure 6). Although these oscillations are also present in the model of Ierley & Miles (2001), they have not been observed in any of the numerical or experimental studies we consider here. In Appendix we demonstrate that these oscillations are generic to the class of rapid-distortion model considered here, if the decay scale in the function $\mathscr{I}$ is not sufficiently long, by using a toy model. In other words, a possible reason for the occurrence of oscillations in the RDT predictions is that the value for z_t obtained from equating the eddy turnover and advection time scales, $T_t(z_t) = T_a(z_t)$, is too small. In fact, since this is only obtained from a scaling argument, a more general but equally valid requirement would be $T_t(z_t) = \gamma T_a(z_t)$, where γ is an $O(1)$ constant. Rather than trying to find an optimum value for γ that would just suppress the oscillations, we note that the predictions for the phaseshift in the wall stress obtained with the

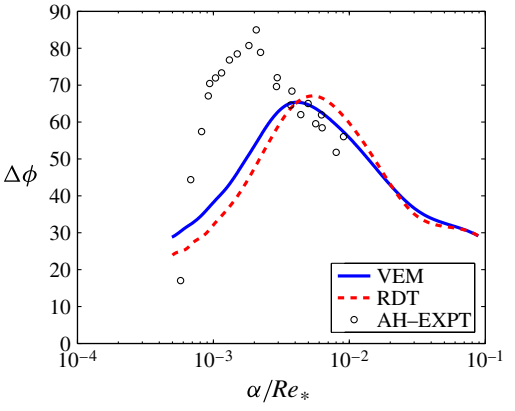

FIGURE 5. The effects of rapid distortion on the phaseshift of the shear stress relative to the wavy wall. The experimental data shown for comparison come from the paper of Abrams & Hanratty (1985).

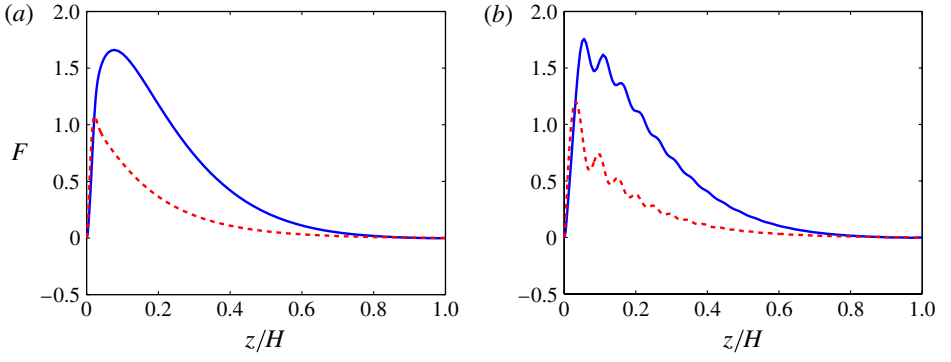

FIGURE 6. Rapid-distortion model: sensitivity study of the effect of the decay length scale of $\mathscr{I}$ on the stream function ($Re_* = 1200$). Solid line, $\Re(\hat{F})$; broken line, $\Im(\hat{F})$. (*a*) The length scale z_t is set according to (3.2); (*b*) the length scale is given by $z_t = \infty$, that is, we have returned to the viscoelastic picture.

viscoelastic and RDT models are in reasonable agreement, and therefore concentrate on the viscoelastic model for the remainder of the paper.

In the viscoelastic model, the only two terms for which closure hypotheses are invoked are the wave-induced dissipation and the viscoelastic relation, wherein $\tilde{\tau}$ is related linearly to $\tilde{k}$. Our assumption for the wave-induced dissipation (2.50) and (2.51) is an approximation based on dimensional analysis; better agreement between theory and experiment can be obtained by modifying this form (e.g. figure 7). Although the viscoelastic relation $\tilde{\tau} = (\tau_0/k_0)\tilde{k}$ is based on a standard treatment, such an approach is valid only in the equilibrium layer of the turbulence, wherein the mean state is characterized by the logarithmic profile. There is no reason to assume that it holds in the limit as $\eta \to 0$. Thus, the correct viscoelastic relation ought to read

$$\tilde{\tau} = \left(\frac{\tau_0}{k_0}\tilde{k}\right) \Psi(\eta; \alpha, Re_*), \tag{3.3}$$

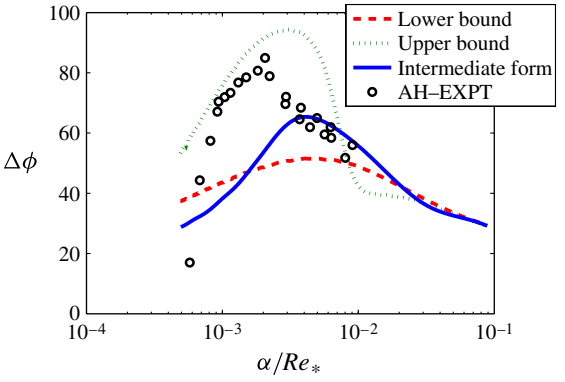

FIGURE 7. Sensitivity analysis for the dissipation function. The upper bound corresponds to the upper bound for the mixing length, $\ell_0 \leqslant H/2$; the lower bound corresponds to a lower estimate for the mixing length $\ell_0 \geqslant d_* = \nu/U_*$. The intermediate form corresponds to the dissipation function $\tilde{\mathscr{E}} = C_D U_0'(\eta)\tilde{k}$. The correct form of the dissipation function is unknown, and the results demonstrate great sensitivity to this function.

where

$$\lim_{\eta\to 0} \Psi(\eta) \propto \mathrm{e}^{-\mathrm{i}\pi/2}, \tag{3.4}$$

to agree with (2.35), and where

$$\lim_{\eta\to\infty} \Psi(\eta) = 1. \tag{3.5}$$

This concept is similar to the notion in 'Model D' that the characteristics of the turbulent stresses change abruptly in the viscous sublayer. We have experimented with several forms for Ψ and better agreement between theory and experiment can be obtained for the quantities plotted in figure 3. However, instead of focusing on optimizing fitting parameters, we note that our unadjusted model gives good qualitative agreement with the experiments of Hanratty and co-workers, and is superior to the other *ab initio* theories developed therein (eddy viscosity, frozen turbulence, k–ϵ model). Further improvement to the model results could also be obtained by using a second-order closure scheme for the WIRSs, as in the work of Meirink & Makin (2000). However, this approach is cumbersome to implement analytically, and we therefore persevere with the simpler method, which gives approximate agreement with the experiments.

3.2. *Comparison with numerical simulations*

We demonstrate, by comparison with DNS, that the viscoelastic model correctly predicts the magnitude of the WIRSs. The comparison is based on the numerical study of Kihara *et al.* (2007), who provide such statistics. We start with the following moving-frame momentum-balance equation

$$\mathscr{L}(\overline{\boldsymbol{u}} \cdot \boldsymbol{\nabla}\overline{u}) = -\frac{\partial \overline{p}}{\partial x} + \frac{\partial \overline{T}_{ix}}{\partial x_i} + \frac{\partial \tau}{\partial z}, \tag{3.6}$$

and we examine the importance of the wave-induced advection, viscous and Reynolds-stress terms relative to the wave-induced pressure term. Here $\mathscr{L}$ represents the linearization of the advective term such that no harmonics are present, and $\overline{T}_{ij}$ is

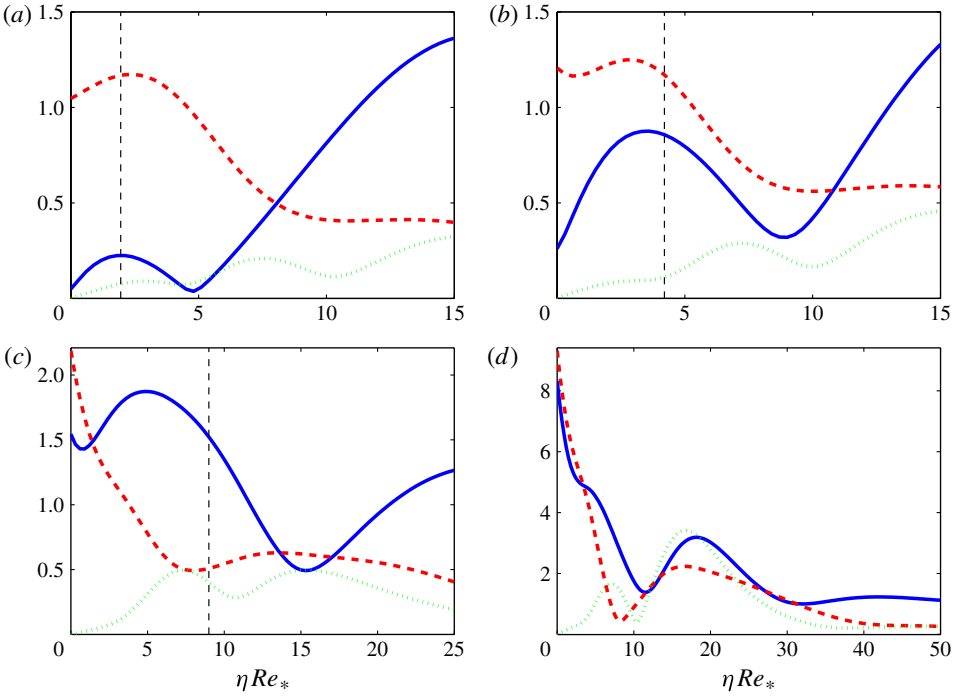

FIGURE 8. Comparison with the work of Kihara *et al.* (2007): vertical profiles of the magnitude of the wave-induced contributions to the streamwise momentum equation, normalized relative to the wave-induced pressure gradient. Solid line: advective term; dashed line: viscous term; dotted line: WIRSs.

the viscous stress tensor. We plot the absolute value of the wave-induced terms, normalized by the wave-induced pressure gradient. The results are shown in figure 8. Unlike in other sections (§§ 3.1 and 4), it is not possible to implement direct comparisons with the DNS: Kihara *et al.* (2007) do not explain how they pass from boundary-fitted coordinates to Cartesian coordinates, and we are therefore unable to map our results directly on to theirs. Nevertheless, a qualitative comparison between figure 8 and figure 12 of the work of Kihara *et al.* (2007) is possible. Our model predicts well the relative importance of the WIRSs, as well as the location of the maxima and minima of this contribution, relative to the critical-layer height. The exact details are not predicted very well: as in § 3.1, our closure model contains several approximations and is inexact. Finally, the model predicts the sign and magnitude of the form drag, compared with the DNS; this is discussed in more detail in the context of shear-driven channel flow. In the context of shear flow again, we discuss the accuracy with which our model predicts the mean, wave-induced flow.

4. Shear-driven channel flows: comparison with simulations

We examine the work of Sullivan *et al.* (2000), who carried out DNS in a shear-driven channel at $Re = 8000$. First, we examine the DNS values of the phaseshift of the wall shear stress and the pressure relative to the wavy wall, using a hierarchy of models. These quantities are important, since the stresses acting on the wavy wall will provide a source of energy to the wave-induced perturbations, if the phaseshifts

c/U_*	DNS	QL	EVM	VEM	RDT	c/U_*	DNS	QL	EVM	VEM	RDT
0	0.5	0.7	0.7	0.7	0.7	0	2.9	2.8	2.8	2.8	2.8
3.9	0.6	0.9	0.9	0.9	0.9	3.9	0.9	1.7	1.8	1.5	1.5
7.8	2.1	2.0	1.9	1.9	1.9	7.8	2.2	2.2	2.0	2.2	2.2
11.5	2.3	2.3	2.3	2.3	2.3	11.5	2.6	3.1	2.9	2.9	2.9
22.0	2.4	2.3	2.4	2.2	2.2	22.0	3.1	3.1	3.1	3.1	3.1

TABLE 1. Parametric study as a function of wave speed c/U_* for $\alpha/Re_* = 0.0262$ with the DNS results of Sullivan *et al.* (2000). The study shows a comparison of the predicted phaseshift $\Delta\varphi = \alpha\Delta x$ between (left) the viscous stress at the wall and the wavy wall; (right) the pressure at the wall and the wall itself.

take certain values. In two-phase flow (§ 5), these energy sources become a route to instability. The wall shear stress is given by (2.24), while the wave-induced pressure can be calculated from the stream function $\hat{F}(\eta)$ in a standard fashion. Although the DNS results show a nonlinear response, the first harmonic clearly dominates, and this comparison is justified: we compute a phaseshift by measuring the distance Δx between the global minimum of the stress and the global minimum of the wall height. We compute the phaseshift for the four models: the results are shown in table 1. The comparison between the DNS and the theory is excellent for the wall shear stress, where the response of the flow to the wavy wall is linear. The comparison is spoiled somewhat in the case of the pressure response, where the response of the pressure to the wavy wall exhibits contributions from higher-order harmonics. To understand the structure of the wave-induced flow, we compare our results for the total stream function (2.16) in boundary-fitted coordinates with figure 16 of Sullivan *et al.* (2000) (figure 9). We use the QL version of our model; the other variants yield similar patterns and are not reported here. Very good qualitative agreement is obtained between the theoretical results and the DNS. Next, we study the wave-induced velocities (figures 10–13), which can be compared in a quantitative way with figures 17–20 in Sullivan *et al.* (2000). These figures show good agreement between the theoretical results and the DNS. These results are insensitive to the turbulent closure hypothesis, and the other models (EVM, VEM etc.) produce similar behaviour. Any small discrepancies between the theoretical and numerical curves can be explained by the nonlinear nature of the simulations.

To explain the fact that all models yield similar results, we examine the relative importance of the advective, viscous and Reynolds-stress terms in the streamwise momentum equation, compared with the pressure gradient, in the VEM framework. A comparison between DNS and our model for the pressure-driven case has already yielded good qualitative agreement (§ 3.2), and suggests that our model is effective in estimating the magnitude of the Reynolds-stress terms. Figure 14 shows the model prediction for the magnitude of the WIRSs. This term contributes very little to the momentum balance, at all wave speeds. Increasing the Reynolds number to a value exceeding that in the DNS ($Re = 10^5$, $Re_* = 2186$, $\alpha/Re_* = 0.0022$) does little to change this balance. Thus, in contrast to the pressure-driven case, where the WIRS is comparable in magnitude to the advective term, in the shear-driven case, the WIRS is relatively unimportant, even at large Reynolds numbers and high wave speeds.

In the preceding figures (figures 10–13), we have indicated the location of the critical layer $U_0(z_c) = c$. Sullivan *et al.* (2000) argued on the basis of stream function plots akin to figure 9 that the Miles mechanism may be important at the intermediate

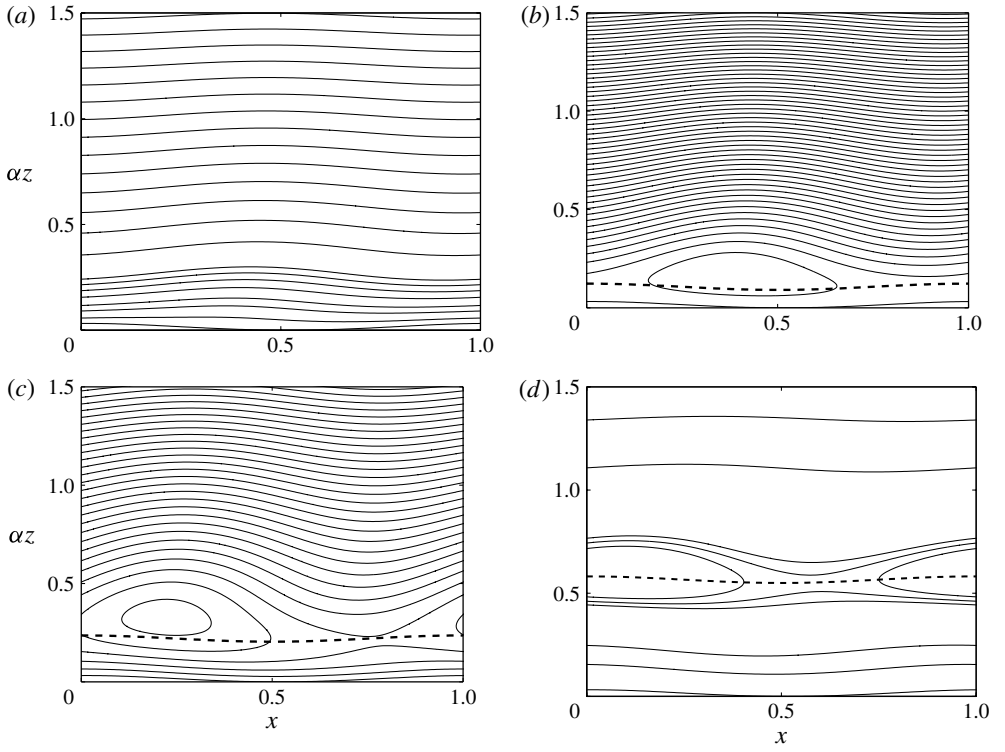

FIGURE 9. Qualitative comparison with the DNS data of Sullivan *et al.* (2000) for $Re = 8000$ (shear-driven single-phase channel flow). The total stream function ψ is shown in each case, with a choice of contours that is designed to highlight the recirculation zone for the two intermediate cases. This is the so-called 'cat's eye' that is responsible for the Miles or critical-layer instability in genuine two-phase flow (see § 5). The critical layer is marked by a broken line: (*a*) $c/U_* = 0$; (*b*) $c/U_* = 3.9$; (*c*) $c/U_* = 7.8$; (*d*) $c/U_* = 11.5$.

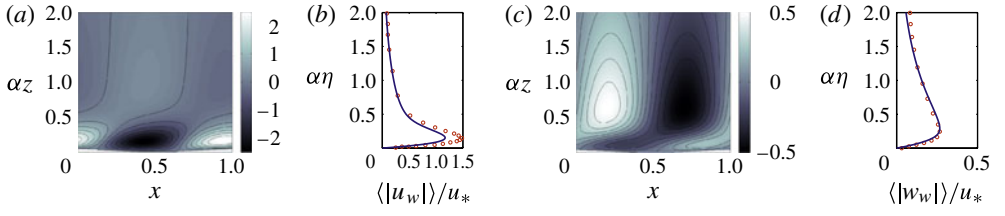

FIGURE 10. Comparison with the DNS data of Sullivan *et al.* (2000) for $Re = 8000$ (shear-driven single-phase channel flow), $c = 0$. (*a*) The wave-induced velocity u_w; (*b*) the streamwise-averaged velocity $L_\xi^{-1}\int_0^{L_\xi} \mathrm{d}\xi\,|\tilde{u}|$ (the solid line comes from our theory; the dots come from the DNS); (*c*) the wave-induced velocity w_w; (*d*) the streamwise-averaged velocity $L_\xi^{-1}\int_0^{L_\xi} \mathrm{d}\xi\,|\tilde{w}|$.

value of $c/U_* = 7.8$, as a cat's eye pattern appeared at the critical height and the critical height is only in the gas and not far removed from the wall at this intermediate case. The present analysis allows us to re-examine this issue rigourously, by writing down an energy decomposition for the wave. Because the QL description agrees so well with the DNS data, we restrict ourselves to this case. We work in the laboratory

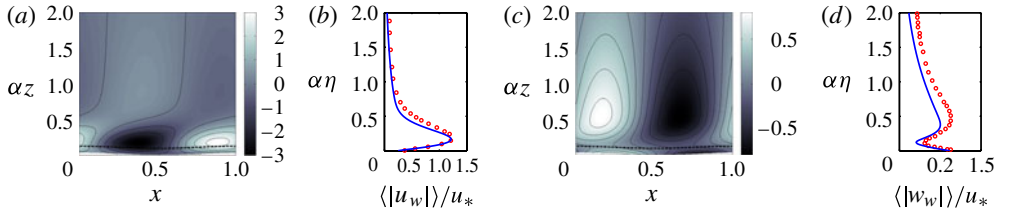

FIGURE 11. The same as figure 10, with $c/U_* = 3.9$. The critical layer, where $U_0(z_c) = c$, is marked by a broken line.

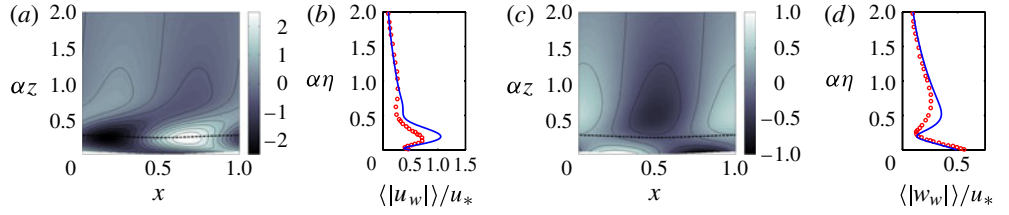

FIGURE 12. The same as figure 10, with $c/U_* = 7.8$. The critical layer, where $U_0\,(z_c) = c$, is marked by a broken line.

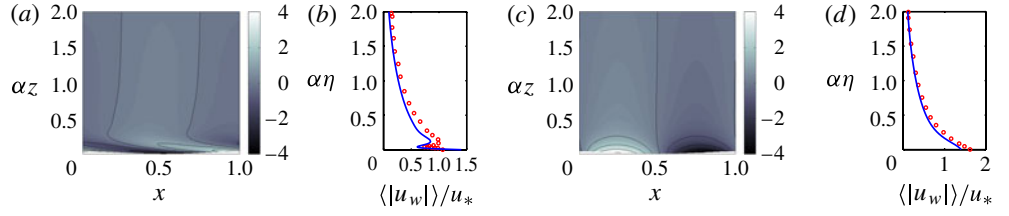

FIGURE 13. The same as figure 10, with $c/U_* = 22$.

frame: we take the dot product of the velocity $\overline{\boldsymbol{u}}$ with the linearized RANS equations and integrate over the periodic cell. The result is the following balance law:

$$KIN + DISS = REY + FIN + TURB + NOR + TAN - \lambda \int_0^1 \mathrm{d}\eta\, U_0'(\eta)\tau_0(\eta) + \lambda \rho_G U_*^2, \tag{4.1a}$$

where $\lambda = 2\pi/\alpha$ and

$$KIN = \frac{1}{2}\frac{\partial}{\partial t}\int_0^{\lambda} \mathrm{d}x \int_{h_0(x-ct)}^1 \mathrm{d}z\, \rho_G \overline{\boldsymbol{u}}^2, \tag{4.1b}$$

$$DISS = \frac{1}{Re}\int_0^{\lambda} \mathrm{d}x \int_{h_0(x-ct)}^1 \mathrm{d}z [2\overline{u}_x^2 + 2\overline{w}_z^2 + (\overline{u}_z + \overline{w}_x)^2], \tag{4.1c}$$

$$REY = -\int_0^1 \mathrm{d}\xi \int_0^1 \mathrm{d}\eta\, \tilde{u}\tilde{w} U_0'(\eta), \tag{4.1d}$$

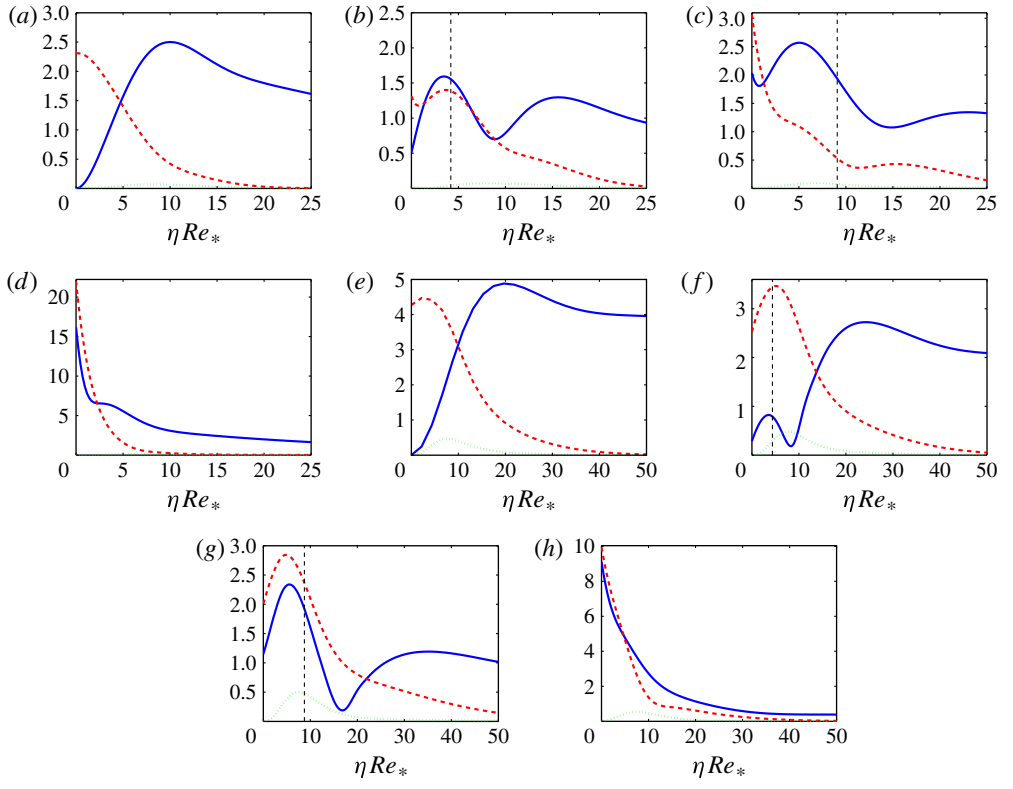

FIGURE 14. The magnitude of the advective, viscous and Reynolds-stress terms, compared with the pressure gradient (solid line, broken line and dotted line, respectively). Across the top: $Re = 8000$; across the bottom: $Re = 10^5$; (*a*) $c/U_* = 0$; (*b*) $c/U_* = 3.9$; (*c*) $c/U_* = 7.8$; (*d*) $c/U_* = 22$; (*e*) $c/U_* = 0$; (*f*) $c/U_* = 3.9$; (*g*) $c/U_* = 7.8$; and (*h*) $c/U_* = 22$.

$$FIN = -\int_0^1 \mathrm{d}\xi \int_0^1 \mathrm{d}\eta [U_0(\eta)\tilde{w}(\widetilde{\partial_z u} + \widetilde{\partial_x w}) - 2a\alpha U_0(\eta)U_0'(\eta)\Re(\Phi)\tilde{w}], \tag{4.1e}$$

$$TURB = -a\alpha \int_0^1 \mathrm{d}\xi \int_0^1 \mathrm{d}\eta\, \tilde{u}\Phi\tau_0'(\eta) + 4a^2\alpha^2 \int_0^1 \mathrm{d}\xi \int_0^1 \mathrm{d}\eta [\Re(\Phi)]^2 U_0(\eta)\tau_0'(\eta), \tag{4.1f}$$

$$NOR = -c\int_0^\lambda \mathrm{d}x \frac{\partial h_0}{\partial x}\left[\tilde{p} + \frac{2}{Re}\widetilde{\partial_{xx} u}\right], \tag{4.1g}$$

$$TAN = -\frac{1}{2}\frac{a^2\alpha^2}{Re}cU_0'(0) - \alpha c\int_0^\lambda \mathrm{d}x\, \widetilde{T_{xz}} h_0(x), \tag{4.1h}$$

where the boundary conditions correspond to an Airy wave. The term *KIN* represents the change in the system's kinetic energy. The sources of energy into the system (e.g. shear at the upper plate, or a streamwise pressure drop) balance with the molecular dissipation (described by the term *DISS*). Hence, the time average of *KIN* is zero. The quantity *REY* represents a transfer of energy from the mean flow into the wave-induced flow, associated with motions in the bulk. The term *FIN* has a similar interpretation, and arises from the finite amplitude of the waves. The second contribution to this term occurs because the volume element itself has multiple

c/U_*	0	3.9	7.8	11.5	22
REY	−0.0321	−0.0341	−0.0098	0.0108	0.0311
FIN	0.1645	0.3109	0.4273	0.0138	0.0013
TURB	−0.0044	−0.0038	0.0016	0.0019	0.0013
TAN	0	−0.0095	0.0055	0.0215	0.1573
NOR	0	−0.0710	−0.1436	−0.0057	0.0726

TABLE 2. Energy budget for the shear-driven case, QL model. Significant contributions to the budget are underlined.

contributions:

$$\mathrm{d}x\,\mathrm{d}z = \{1 - 2\alpha a\Re(\Phi) + 4\alpha^2 a^2[\Re(\Phi)]^2\}\,\mathrm{d}\xi\,\mathrm{d}\eta. \tag{4.2}$$

Finally, *NOR* and *TAN* represent the transfer of energy into the wave-induced flow as a result of normal and tangential stress at the bottom wall. The results of the decomposition are shown in table 2. The dominant source of energy balancing the dissipation varies as a function of wave speed c/U_*. For $c \neq 0$, the terms *REY*, *FIN* and *TAN* are of particular interest. The term *REY* is unimportant for all but the intermediate value $c/U_* = 11.5$. The term *TAN* is initially negative but becomes positive, and dominates as an energy source for large c/U_* values, $c/U_* \geqslant 11.5$. For the intermediate c/U_* values, the terms *REY* and *FIN* when taken together, dominate as the energy source. In the context of interfacial instability of waves of infinitesimally small amplitude, the dominance of the term *REY* is the signature of a critical-layer or Miles-type instability (Boomkamp & Miesen 1996): its pre-averaged form has a large contribution at the critical layer, associated with energy transfer into the perturbations. Although this scenario is distinct from the situation considered here (waves of infinitesimally small slope), the positivity of *REY* suggests that the critical layer is playing a role as an energy source. This parallelism between interfacial instability and the flow disturbance past a wavy wall is strengthened by consideration of the functions

$$\tau_{wrs}(\eta) = -\int_0^\lambda \mathrm{d}\xi\ \tilde{u}\tilde{w}, \tag{4.3a}$$

$$\tau_{fin}(\eta) = -\int_0^\lambda \mathrm{d}\xi\ \left[\frac{U_0}{U_0'}\tilde{w}(\widetilde{\partial_z u} + \widetilde{\partial_x w}) - 2a\alpha U_0\Re(\Phi)\tilde{\eta}\right], \tag{4.3b}$$

such that

$$REY = \int_0^1 \mathrm{d}\eta\ \tau_{wrs}(\eta)U_0'(\eta), \quad FIN = \int_0^1 \mathrm{d}\eta\ \tau_{fin}(\eta)U_0'(\eta). \tag{4.3c}$$

(The subscript 'wrs' denotes the wave Reynolds stress.) For infinite Reynolds numbers, it is known that the function $\tau_w(\eta)$ possesses a jump across the critical layer $U_0(\eta_c) = 0$, signifying an energy source (Miles 1957; Benjamin 1959). For the finite Reynolds numbers considered here, we expect $\tau_{wrs}(\eta)$ to change sign near $\eta = \eta_c$, again signifying an energy input (Boomkamp & Miesen 1996). This is visible clearly in figure 15: for intermediate c/U_* values ($c/U_* = 3.9, 7.8, 11.5$), the wave Reynolds stress is positive below the critical layer, indicating a net input of energy into the waves; the function has a zero at $\eta = \eta_c$ and beyond $\eta = \eta_c$, the wave Reynolds stress is negative.

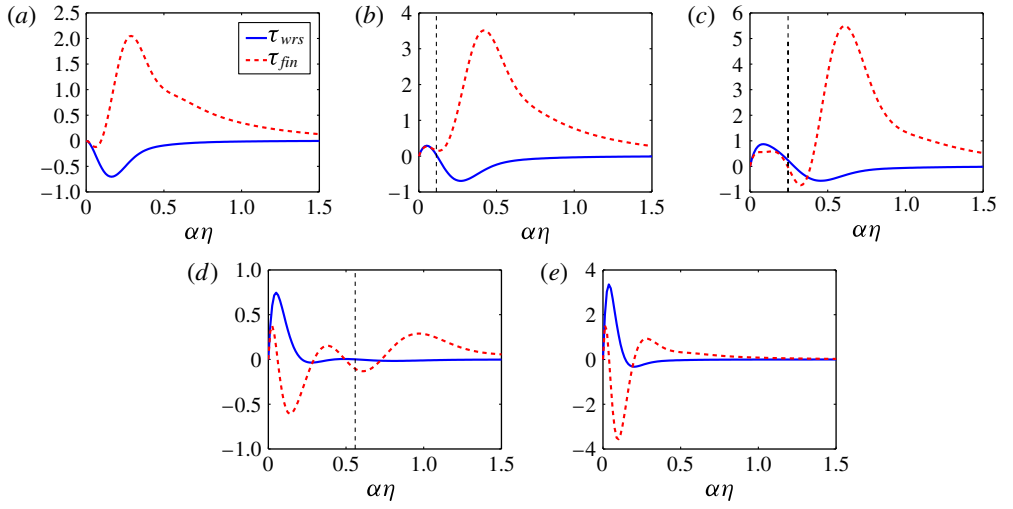

FIGURE 15. The wave Reynolds stress function and the analogous finite-amplitude stress function, as a function of wave speed: (*a*) $c/U_* = 0$; (*b*) $c/U_* = 3.9$; (*c*) $c/U_* = 7.8$; (*d*) $c/U_* = 11.5$; and (*e*) $c/U_* = 22$.

Note that the critical-layer mechanism acts only at intermediate c/U_* values: if c/U_* is small, the critical layer lies close the surface, the mean-flow curvature is negligible, and the mechanism does not operate (Miles 1957); If c/U_* is large, then the critical layer lies far from the surface, and it cannot interact with the wave-induced flow. These results highlight the central role of the critical layer in the generation of energy inputs to the perturbations, and underscore the contention of Sullivan *et al.* (2000) that the critical layer is dynamically important. As c/U_* increases, the contribution to the energy sources from the interfacial terms *TAN* and *NOR* become important, until at $c/U_* = 22$, it is the *TAN* term that dominates. Again, this is consistent with our knowledge of the instability of genuine interfaces (as opposed to wavy walls): for several canonical instabilities, it is this term that provides a net source of energy into the system (Boomkamp & Miesen 1996).

We comment on the lack of involvement of the so-called 'form drag'

$$D_p = \int_0^\lambda \mathrm{d}x\, p \frac{\partial h_0}{\partial x} \tag{4.4}$$

in this calculation. The coefficient D_p can be brought into the calculation by rearrangement of the energy budget (4.1):

$$cD_p = \left\langle REY + FIN + TAN + TURB - 2cRe^{-1} \int_0^\lambda \mathrm{d}x\, \widetilde{\partial_{xx} u} - DISS \right\rangle$$
$$- \lambda \int_0^1 \mathrm{d}\eta\, U_0'(\eta)\tau_0(\eta) + \lambda \rho_G U_*^2, \tag{4.5}$$

where the ensemble average $\langle\cdot\rangle$ herein reduces to a time average, such that $\langle KIN \rangle = 0$. This re-arrangement sheds no light on the mechanisms by which energy is delivered into the wave-induced flow: all terms in the energy budget are necessary to this understanding. This conclusion is especially relevant to genuine *interfacial* instability, in which case we must also solve the stability problem in the liquid and so determine the growth rate. This is the subject of § 5.

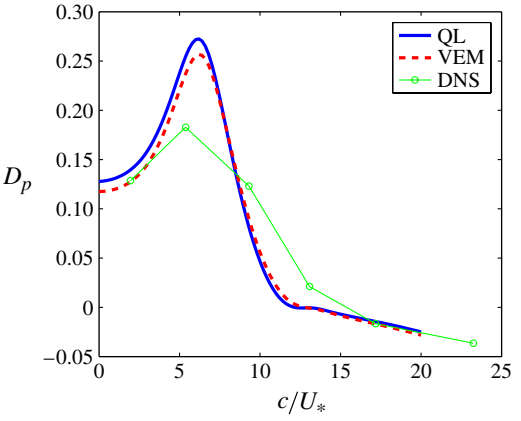

FIGURE 16. Comparison between the theoretical form-drag parameter and DNS. Solid line: QL; dotted line: VEM; datapoints: DNS of Sullivan *et al.* (2000). The difference between the QL and EVM descriptions is not significant. Both models predict negative values of β at large wave speeds, consistent with non-separated sheltering by (molecular) viscous effects.

Although we have demonstrated the unimportance of the form drag in pinpointing the source of instability, it is helpful to use it in validating our theories against DNS. Thus, we compute D_p and show comparisons with the DNS in figure 16. There is little difference between the QL and viscoelastic descriptions. Both descriptions provide for a negative value of β at large wave speeds. This is consistent with the DNS but inconsistent with the purely inviscid Miles theory. Thus, it is the ordinary molecular viscosity, and not the contribution of turbulent stresses, that plays a role in generating negative D_p-values at large wave speeds. This is consistent with Benjamin's theory of viscosity-induced non-separated sheltering (Benjamin 1959) (but see also the paper of Boomkamp *et al.* 1997).

In view of these considerations, the approximate agreement between DNS and theory obtained in this section is satisfactory. We therefore pass over to turbulent flow in the case of genuine two-phase flow, where we examine the dynamics of both the liquid and the gas layers.

5. Deep-water waves

Having analysed turbulent flow over a moving wavy wall, we now proceed to extend this study to turbulent gas flow over a liquid layer, resolving the wave-induced flow in the liquid as well as in the gas. Unlike in previous sections, we consider herein waves of infinitesimally small amplitude. In practical applications (Cohen & Hanratty 1965; Craik 1966; Hewitt & Hall-Taylor 1970), the wave speed is not a parameter and must be determined by solving an eigenvalue analysis. This analysis is based on solving an equation for the stream function in both phases and applying matching conditions at the interface. We focus on the shear-driven case, with coupling to a deep liquid layer. We expect the WIRSs to be of marginal importance; nevertheless, we continue to investigate this issue, using the viscoelastic formulation. The physical scenario just described has been investigated previously (Miesen & Boersma 1995; Boomkamp & Miesen 1996; Özgen, Degrez & Sarma 1998), without the modelling of the WIRSs.

We study the case of a shear-driven turbulent gas, coupled across an interface to a liquid flow. Thus, the flow is confined by a flat plate at $z = H$, a large distance from

the interface. This plate moves at velocity U_{max} relative to the interface. Thus, the basic velocity is unchanged from (2.4), the Reynolds number is based on the upper-plate velocity $Re = \rho_G U_{max} H/\mu_G$, and the friction Reynolds number $Re_* = \rho_G U_* H/\mu_G$ is fixed by the condition

$$\frac{Re_*^2}{Re}\int_0^1 \frac{\mathrm{d}s}{1+\kappa Re_* s(1-s)f(s)f(1-s)} = 1. \tag{5.1}$$

The flow in the gas is coupled to a non-dimensional flow profile in the liquid:

$$U_0(z) = A(\mathrm{e}^{Bz} - 1), \quad z < 0, \tag{5.2}$$

where A and B are constants to be determined. This model has been used before by (Boomkamp & Miesen 1996) and by Zeisel, Stiassnie & Agnon (2007). Equation (5.2) contains only one free parameter, since the continuity of tangential stress requires

$$mU_0'(0-) = U_0'(0+), \quad z = 0, \tag{5.3}$$

where $m = \mu_L/\mu_G$ is the viscosity ratio. Hence, $mAB = Re_*^2/Re$, and there remains a single free constant A whose value is fixed with reference to the literature (Boomkamp & Miesen 1996), $U_0(0)/U_* = O(1)$, hence $A = Re_*/Re$. Thus,

$$U_0(z) = \frac{Re_*}{Re}\left[\exp\left(\frac{z\,Re_*^2}{mA\,Re}\right) - 1\right], \quad z < 0. \tag{5.4}$$

Next, we focus on the wave-induced component of the velocity, in a manner similar to § 2. Now, however, we assume an infinitesimal wave amplitude. Thus, in a standard fashion (Valluri *et al.* 2010), the wave-induced stream function in liquid layer ($\widetilde{\psi}_L$) obeys

$$\mathrm{i}\alpha r[(U_0 - c)(\partial_z^2 - \alpha^2)\widetilde{\psi}_L - U_0''\widetilde{\psi}_L] = m\,Re^{-1}(\partial_z^2 - \alpha^2)^2\widetilde{\psi}_L, \quad z \leqslant 0, \tag{5.5a}$$

where $\rho = \rho_L/\rho_G$ is the density ratio. The wave-induced stream function in gas layer ($\widetilde{\psi}_G$) obeys

$$\mathrm{i}\alpha[(U_0 - c)(\partial_z^2 - \alpha^2)\widetilde{\psi}_G - U_0''\widetilde{\psi}_G] = Re^{-1}(\partial_z^2 - \alpha^2)^2\widetilde{\psi}_G + (\partial_z^2 + \alpha^2)\widetilde{\tau}. \tag{5.5b}$$

The equation for the TKE is

$$\begin{aligned}[\mathrm{i}\alpha(U_0 - c) + C_D U_0']\widetilde{k} = {} & (Re^{-1} + \mu_T)(\partial_z^2 - \alpha^2)\widetilde{k} + \mu_T'\partial_z\widetilde{k} + \mu_T''\widetilde{k} \\ & + U_0'\widetilde{\tau} + \tau_0(\partial_z^2 + \alpha^2)\widetilde{\psi}_G + \mathrm{i}\alpha k_0'\widetilde{\psi}_G,\end{aligned} \tag{5.5c}$$

and the stress $\widetilde{\tau}$ is accounted for either by the viscoelastic theory, or the rapid-distortion theory discussed in § 2. Across the interface, the stream function satisfies the conditions of continuity of velocity and tangential stress, and the jump condition in the

normal stress:

$$\widetilde{\psi_L} = \widetilde{\psi_G}, \tag{5.6a}$$

$$\partial_z\widetilde{\psi_L} = \partial_z\widetilde{\psi_G} + \frac{\widetilde{\psi_L}}{c - U_0(0)}[U_0'(0+) - U_0'(0-)], \tag{5.6b}$$

$$m(\partial_z^2 + \alpha^2)\widetilde{\psi_L} = (\partial_z^2 + \alpha^2)\widetilde{\psi_G} + Re\,\widetilde{\tau}, \tag{5.6c}$$

$$\begin{aligned} m(\partial_z^3\widetilde{\psi_L} - 3\alpha^2\partial_z\widetilde{\psi_L}) + \mathrm{i}\alpha r\,Re[c - U_0(0)]\partial_z\widetilde{\psi_L} + \mathrm{i}\alpha r\,Re\,U_0'(0-)\widetilde{\psi_L} \\ = (\partial_z^3\widetilde{\psi_G} - 3\alpha^2\partial_z\widetilde{\psi_G}) + \mathrm{i}\alpha\,Re[c - U_0(0)]\partial_z\widetilde{\psi_G} + \mathrm{i}\alpha\,Re\,U_0'(0+)\widetilde{\psi_G} \\ + \partial_z\widetilde{\tau} + \frac{\mathrm{i}\alpha r\,Re}{c - U_0(0)}(Fr + \alpha^2 S)\widetilde{\psi_G}, \end{aligned} \tag{5.6d}$$

where we have introduced the inverse Froude and inverse Weber numbers, respectively,

$$Fr = \frac{g(\rho_L - \rho_G)H}{\rho_G U_{max}^2}, \quad S = \frac{\sigma}{\rho_G U_{max}^2 H}. \tag{5.7}$$

Here g and σ denote gravity and surface tension, respectively. The TKE equation is second order, and therefore requires only two boundary conditions. We apply the conditions $k_0 + \tilde{k} = 0$ on the small-amplitude free surface and on $z = 1$, the non-dimensional vertical extent of the gas layer. These conditions are based on the assumption that the gas-phase turbulence 'sees' the interface as a solid wall. The validity of this assumption is examined below. Upon linearization on to the surface $z = 0$, these kinetic energy conditions are

$$\widetilde{k} = 0 \quad \text{at } z = 0, \text{ and at } z = 1. \tag{5.8}$$

Consequently, $\tilde{\tau} = 0$ in (5.6*c*), and the interfacial conditions (5.5) reduce to the standard form seen in laminar flow (Valluri *et al.* 2010). Finally, at the top of the gas domain $z = 1$, we have the requirement that the perturbation velocities should vanish:

$$\widetilde{\psi_G} = \partial_z\widetilde{\psi_G} = 0. \tag{5.9}$$

Thus, we obtain a total of 10 conditions, which provides sufficient information to close the system of equations $(\widetilde{\psi_L}, \widetilde{\psi_G}, \widetilde{k}, \widetilde{\tau})$. No conditions are required on $\widetilde{\tau}$, since it appears only in an algebraic way in the model. We solve (5.4)–(5.9) using a Chebyshev collocation method, which is augmented to include the kinetic energy and the stress (for a description and validation of this method, see Valluri *et al.* 2010). Following standard practice, we modify the number of collocation points until convergence is achieved: for $Re = 10^5$, 300 collocation points in the liquid (N_L) and 150 points in the gas (N_G) are sufficient for convergence to four significant figures for $\Re(\alpha c)$ and two significant figures for $\Im(\alpha c)$.

We carry out a linear stability analysis around the base state just described, for the following parameter values:

$$m = 55, \quad r = 1000, \quad Re = 10^5, \quad S = 0 \tag{5.10}$$

and for various Fr numbers. Our parameter choices are based on values relevant to the generation of waves by wind in oceanographic applications (Boomkamp & Miesen 1996). We vary Fr around a reference value $Fr_0 = 500$ because we have found elsewhere that the value of Fr controls the wave speed (Ó Náraigh *et al.* 2011).

Some results concerning the growth rates and wave speeds are shown in figure 17. The value of the inverse Froude number is made to vary around the reference value $Fr_0 = 500$. This is close to the threshold value for which the system becomes stable at all wavenumbers. The dispersion curves for the zero-equation QL and one-equation models are shown in the figure. We focus on the one-equation viscoelastic model (the rapid distortion introduces negligible changes relative to the viscoelastic results: the difference between these curves is so small that we do not show it here). The results for the QL and one-equation models are similar in their behaviour, and the quantitative differences are small.

The results of figure 17 are based on the assumption that the gas 'sees' the interface as though it were a solid wall. This is a reasonable assumption for small-amplitude waves in two-phase flows with large density contrasts, as various numerical simulations imply (Lombardi, Angelis & Banerjee 1995; Fulgosi *et al.* 2002; Lin *et al.* 2008). Thus, in our base-state model $k_0 \sim z^2$ as the interface $z = 0$ is approached, in accordance with wall flows. Nevertheless, these works clearly point out that the actual value of $k_0(0)$ at the interface, while small, is not zero. To understand the effects of such coupling on the stability results, we have extended the viscoelastic model to the liquid phase, and linked the turbulence in the different phases by prescribing a non-zero value for $k_0(0)$ at the interface. This value cannot be determined *a priori*, and is therefore treated as a free parameter, which we vary. Specifically, we take

$$k_0(0) = \varepsilon \rho_G u_{*G}^2, \tag{5.11}$$

and we investigate the effects of this varying ε on the stability analysis. We retain the interfacial condition $\tilde{k} = 0$: numerical studies suggest that the diagonal component of the Reynolds stress tensor vanishes rapidly as the interface is approached (Lombardi *et al.* 1995; Fulgosi *et al.* 2002; Lin *et al.* 2008), hence $\tilde{\tau} = 0$ at the interface, and we are thus forced to retain the interfacial condition $\tilde{\tau} = (\tau_0/k_0)\tilde{k} = 0$. The results of the implementation of this modified model are shown in figure 18. They do not differ very much from the results in figure 17. This consistency between the basic model and the modified one reinforces the robustness of our whole approach. Nevertheless, when we go beyond the assumption of wall–interface interchangeability in the modelling of the turbulent WIRS, we are unable to derive the precise scaling laws for $k_0 \sim k_0(0) + z^{p_1}$ and $\tau_0 \sim z^{p_2}$. It can therefore be said that the modified viscoelastic model discussed herein represents the absolute limit of linear modelling, and that the next necessary step in the description of wave generation by turbulent winds must involve numerical simulations.

The energy-budget analysis for small-amplitude waves in two-phase flow has been developed elsewhere (Boomkamp & Miesen 1996), and is similar to that described in § 4. Such analysis, applied to the cases in figure 17, pinpoints two destabilizing influences:

$$REY_G = \int_0^1 \mathrm{d}z\, \tau_{wrs}(z) U_0'(z), \quad \tau_{wrs}(z) = -\int_0^\lambda \mathrm{d}x\, \tilde{u}\tilde{w}, \tag{5.12}$$

and

$$TAN = \int_0^\lambda \mathrm{d}x [(\widetilde{u_L} - \widetilde{u_G})\widetilde{T_{xz}}]_{z=0} = (m-1)\frac{Re_*^2}{Re}\int_0^\lambda \mathrm{d}x\, \eta(x)\widetilde{T_{xz}}(x, z=0). \tag{5.13}$$

The term REY_G picks up a large contribution close to the critical layer $U_0(z) = c_r$, where the function $\tau_{wrs}(z)$ attains its maximum value. The term TAN is positive if

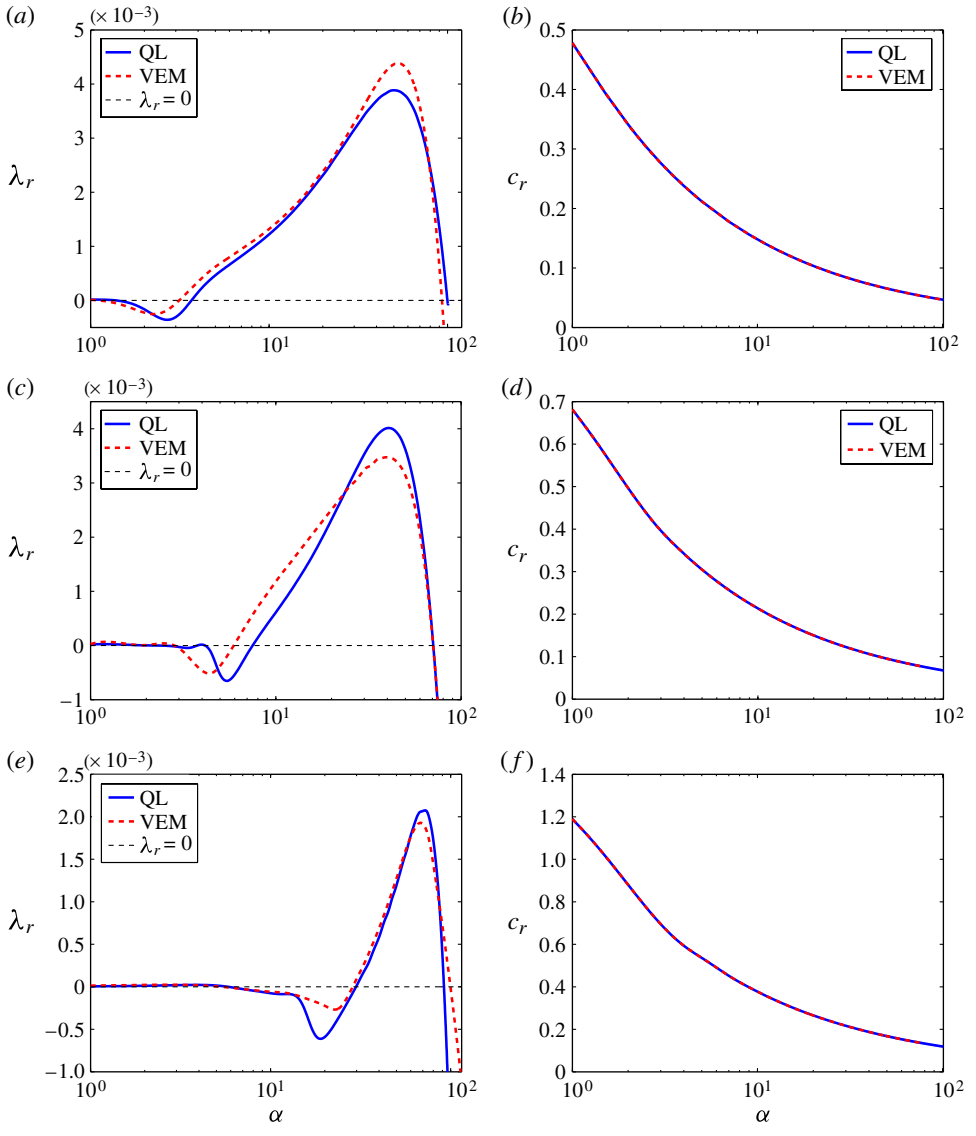

FIGURE 17. Growth rates $\lambda_r = \alpha c_i$ of the linear stability analysis, with reference inverse Froude number $Fr_0 = 500$; the other parameters are determined by (5.10). Left column, growth rates; right column, wave speeds. Across the top, $Fr = 0.5Fr_0$; middle row, $Fr = Fr_0$; across the bottom $Fr = 3Fr_0$.

$m > 1$, and if the absolute value of the phase shift between the free surface and the wave-induced viscous stress is less than $\pi/2$. This underscores the importance of the phaseshift study in any linear stability analysis. In both cases, it is the first term that dominates (see table 3). This is entirely consistent with the finite-amplitude, wavy-wall calculations carried out in § 4. Similar also to § 4 is the functional form of the total stream function, shown at maximum growth in figure 19: there are 'cat's eyes' at the crest of the wave, which is linked to the dominance of the critical-layer mechanism.

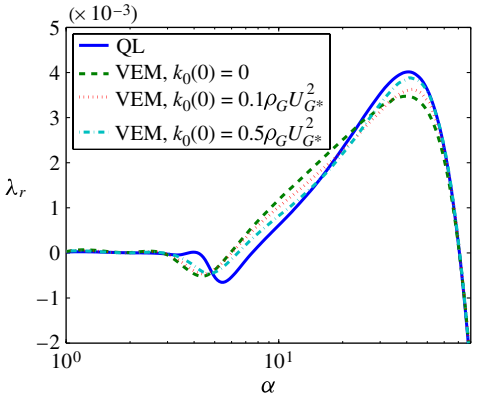

FIGURE 18. Growth rates $\lambda_r = \alpha c_i$ of the linear stability analysis, for the coupled model (VEM in both layers). The wave speeds are the same in all of the models and are not shown. Here $Fr = Fr_0 = 500$.

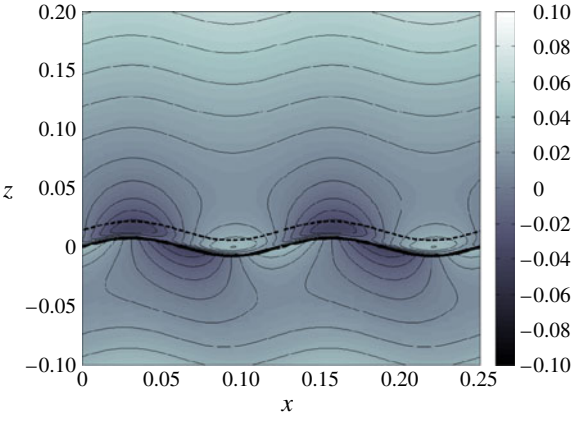

FIGURE 19. Stream function at $\alpha = 39$, $Fr = Fr_0$ (QL model).

	KIN_L	KIN_G	REY_L	REY_G	$DISS_L$	$DISS_G$	$TURB_G$	NOR	TAN
QL	0.99	0.01	−1.70	103.75	−21.63	−102.45	0	−48.24	71.26
VEM	0.98	0.02	−1.50	74.52	−15.00	−62.62	−15.55	−39.41	59.06

TABLE 3. Energy budget for $\alpha = 39$, $Fr = Fr_0$.

The results of a more detailed parametric study are shown in figure 20, wherein we see the effects of the inverse Froude number on the linear stability upon decreasing the inverse Froude number away from criticality (recall that the results in figure 17 are near criticality). The results are similar for the zero- and one-equation models (QL and VEM): decreasing the inverse Froude number is destabilizing and leads to slower waves. The slow waves are in evidence in figure 20(*c*). The change in the stability characteristics is mirrored in the energy budgets, whose values we tabulate for the QL case in table 4. To highlight further the change in the stability characteristics,

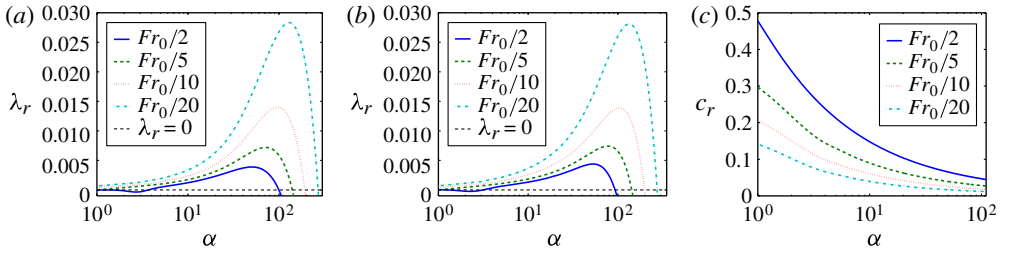

FIGURE 20. Growth rates $\lambda_r = \alpha c_i$ of the linear stability analysis, showing the effects of decreasing Fr, with reference inverse Froude number $Fr_0 = 500$. (*a*) Growth rate in the QL description; (*b*) growth rate in the VEM description; (*c*) wave speed (both turbulence models agree here).

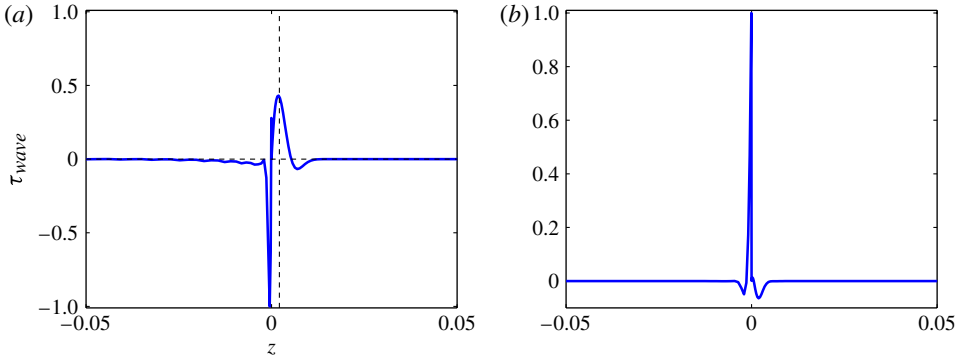

FIGURE 21. Wave Reynolds stress function at maximum growth for (*a*) $Fr = Fr_0$; (*b*) $Fr = Fr_0/20$. In (*a*) the stress function is maximal near the critical layer, $z_c = 0.0021$, suggesting that the critical layer plays a role in the instability; in (*b*) the stress function is maximal at the interface, suggesting an interfacial instability, due to the mismatch in viscosity across the interface.

we study the wave Reynolds stress function at maximum growth for the two extreme cases, $Fr = Fr_0$ and $Fr = Fr_0/20$ (see figure 21). The wave Reynolds stress changes form: in the former case the critical-layer mechanism is clearly important, since the stress function has a maximum close to this point, while in the latter case, this mechanism appears to be unimportant, since the stress function is maximal directly at the interface, underscoring the importance of the *TAN* term in the energy budget, and demonstrating that we have achieved a transition from the critical-layer to the interfacial instability. According to (5.13), this interfacial instability is driven by the mismatch in the viscosity across the interface.

A comparison between our theoretical predictions and experimental results is possible by examination of the quantity

$$\beta = \frac{\text{Maximum growth rate}}{\text{Frequency at maximum growth rate}} = \frac{c_i(\alpha_{max})}{c_r(\alpha_{max})}. \tag{5.14}$$

A review of the experimental data for the generation of wind by waves (Plant 1982) suggests the following empirical bound for β:

$$0.02\left(\frac{U_*}{c_r}\right)^2 \leqslant \beta \leqslant 0.06\left(\frac{U_*}{c_r}\right)^2, \tag{5.15}$$

Fr	REY_L	REY_G	$DISS_L$	$DISS_G$	$TURB$	NOR	INT
Fr_0	−0.02	1.10	−0.36	−1.19	0.00	−0.40	1.00
$(1/2)Fr_0$	−0.01	0.42	−0.32	−0.74	0.00	−0.17	1.00
$(1/5)Fr_0$	0.00	0.07	−0.19	−0.72	0.00	−0.04	1.00
$(1/10)Fr_0$	0.00	−0.02	−0.14	−0.74	0.00	−0.04	1.00
$(1/20)Fr_0$	0.00	−0.07	−0.09	−0.77	0.00	−0.05	1.00

TABLE 4. Energy budget at maximum growth detailing the transition from critical-layer to viscosity-stratified waves, as a function of gravity number, where $Fr_0 = 500$ and $Re = 10^5$. The budgets have been normalized such that $TAN = 1$ in each case. In the first table, we have included the WIRSs; in the second table, they are set to zero.

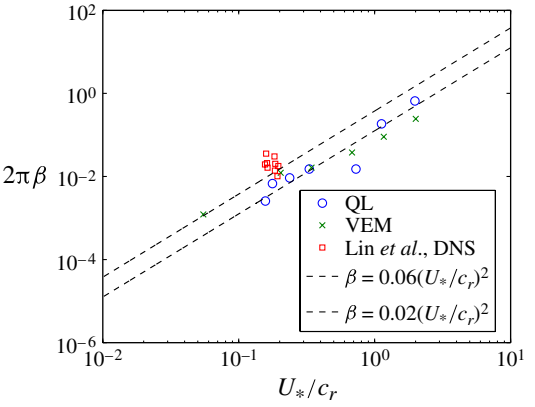

FIGURE 22. Comparison between our models and the experimental correlation of Plant (1982) (dashed lines) and the DNS results of Lin *et al.* (2008) (squares).

where U_* is the interfacial friction velocity. The DNS results of Lin *et al.* (2008) for two-phase interfacial turbulence imply a growth rate β that is within, or slightly above this range (those authors use a model of shear-driven turbulence similar to the model used here). Thus, we plot β as a function of U_*/c_r in figure 22, using both the zero- and one-equation models of turbulence. The results in both cases are within, or close to the formula (5.15) proposed by Plant. Our growth-rate results are also close to the numerical predictions of Lin and coworkers. This close agreement between our theories and the empirical results inspires confidence in our model. It also highlights the marginal role of the WIRSs in general, and rapid distortion in particular, in the generation of waves by wind. The concurrence underscores the crucial role played by the critical layer and the viscosity contrast in the creation of interfacial instabilities. This conclusion is consistent with the recent work of wind–wave interaction (Hristov, Miller & Friehe 2003), whose empirical measurements support the critical-layer mechanism as the means for generating waves on the ocean surface.

6. Conclusions

We have formulated a one-equation model of interfacial turbulence with special emphasis on modelling the interaction between the turbulent stresses and interfacial

Source	System	α/Re_*	Model
Zilker *et al.* (1976)	Wavy wall, $c = 0$	High	QL model suffices
Abrams & Hanratty (1985)	Wavy wall, $c = 0$	Low	One-equation model, dissipation of TKE dominates
Sullivan *et al.* (2000)	Wavy wall, $c \geqslant 0$	High	QL model suffices
This study	Interfacial flow, infinitesimal waves have amplitude	Low	QL model and one-equation model give similar results

TABLE 5. Summary of the systems studied and the applicable models.

undulations. We have applied the model to a variety of test cases (involving both a wavy wall and genuine two-phase flow). These are summarized in table 5, where we also summarize the performance of the models relative to DNS and experiments. In all cases considered, the effects of rapid distortion do not appear to be relevant. In the wavy-wall case (at finite wave amplitude, but small wave slope), the WIRSs play no role at all at low Reynolds numbers, while at higher Reynolds numbers, they are necessary in order for the experimental and theoretical values of the wall shear stress to agree. However, approximate qualitative agreement is possible within the QL framework, even at these higher Reynolds numbers. The solution of the fully coupled two-layer problem (albeit at infinitesimal wave amplitudes) supports this conclusion. More analysis and data are required in order to address the finite-amplitude, small-slope, fully coupled problem. However, given the results on display here, it is unlikely that the WIRSs will play a significant role in the generation of interfacial instability in this more general case. That a cat's eye stream function is visible in both the wavy-wall (finite amplitude) and wavy-interface (infinitesimal amplitude) cases at certain values of the wave speed supports the conclusion that the Miles mechanism of interfacial instability is important. This conclusion appears to be supported by the most recent experimental and theoretical results (Hristov *et al.* 2003; Janssen 2004). Moreover, the stream function information generated in the two-phase case may be of use as a testbed for future DNS studies.

This work has been undertaken within the Joint Project on Transient Multiphase Flows and Flow Assurance. The authors wish to acknowledge the contributions made to this project by the UK Engineering and Physical Sciences Research Council (EPSRC) and the following: Advantica; BP Exploration; CD-adapco; Chevron; ConocoPhillips; ENI; ExxonMobil; FEESA; IFP; Institutt for Energiteknikk; PDVSA (INTEVEP); Petrobras; PETRONAS; Scandpower PT; Shell; SINTEF; StatoilHydro; and TOTAL. The authors wish to express their sincere gratitude for this support. The authors would also like to thank their colleague O. Matar and former colleague C. Lawrence for useful discussions, and K. Tong and M. Wong for their assistance in carrying out the numerical studies.

Appendix. Strange oscillations are generic to rapid-distortion models

As mentioned in § 3, the rapid-distortion theory as constituted in this paper, and in the work of Townsend (1972, 1980) and Ierley & Miles (2001), contains bulk oscillations that are inherent in the model. These oscillations can be damped to zero by

a careful choice of parameters. To understand this in more detail, we consider a simple two-fluid toy model, wherein analytical solutions are possible. This model possesses as its solution the oscillatory far-field structures visible in figure 6.

The toy model consists of the following base state

$$U = \begin{cases} mz, & -1 \leqslant z \leqslant 0, \\ z, & 0 \leqslant z \leqslant b, \\ b, & z \geqslant b, \end{cases} \tag{A 1}$$

together with the following Orr–Sommerfeld and WIRS equations (cf. (5.4) and (5.5)):

$$\mathrm{i}\alpha r(mz - c)(\partial_z^2 - \alpha^2)\widetilde{\psi_L} = m\,Re^{-1}(\partial_z^2 - \alpha^2)^2\widetilde{\psi_L}, \quad -1 \leqslant z \leqslant 0, \tag{A 2a}$$

$$\mathrm{i}\alpha(z - c)(\partial_z^2 - \alpha^2)\widetilde{\psi_G} = Re^{-1}(\partial_z^2 - \alpha^2)^2\widetilde{\psi_G}, \quad 0 \leqslant z \leqslant b, \tag{A 2b}$$

$$\mathrm{i}\alpha(b - c)(\partial_z^2 - \alpha^2)\widetilde{\psi_L} = Re^{-1}(\partial_z^2 - \alpha^2)^2\widetilde{\psi_L} + (\partial_z^2 + \alpha^2)\tilde{\tau}, \quad z \geqslant b, \tag{A 2c}$$

$$\mathrm{i}\alpha(U_0 - c)\tilde{\tau} = -q_\infty(\beta_1\partial_z^2\widetilde{\psi_G} + \beta_2\alpha^2\widetilde{\psi_G} + \mathrm{i}\alpha\beta_3\partial_z\widetilde{\psi_G}), \tag{A 2d}$$

where q_∞ is the *constant* TKE in the far field. Furthermore, we have

$$\beta_1 = 2(\boldsymbol{n}_{12}^{(0)})^2 - (1 - C_R)\boldsymbol{n}_{22}^{(0)}, \tag{A 3a}$$

$$\beta_2 = 2\boldsymbol{n}_{12}(\boldsymbol{n}_{11} - \boldsymbol{n}_{22}), \tag{A 3b}$$

$$\beta_3 = 2(\boldsymbol{n}_{12}^{(0)})^2 - (1 - C_R)\boldsymbol{n}_{12}^{(0)}. \tag{A 3c}$$

Given a set of boundary and interfacial conditions, it is possible to obtain a closed-form solution to this set of equations (Abramowitz & Stegun 1965; Drazin & Reid 1981). Our goal here, however, is simply to elucidate the oscillatory nature of the solution found in the full analysis. To that end, we take a characteristic value of the wave speed c, and obtain a solution to the system (A.2) in the far field $z \geqslant b$. There, the solution is $\widetilde{\psi_G} = \mathrm{e}^{\gamma z}$, where γ solves a fourth-order polynomial equation:

$$\begin{aligned}(1 + \mathrm{i}\beta_1 Re_q)(\gamma/\alpha)^4 - \beta_3 Re_q(\gamma/\alpha)^3 + [\mathrm{i}(\beta_1 + \beta_2)Re_q - 2 - \mathrm{i}\,Re_b](\gamma/\alpha)^2 \\ - \beta_3 Re_q(\gamma/\alpha) + \mathrm{i}\,Re_q\beta_2 + 1 + \mathrm{i}\,Re_b = 0,\end{aligned} \tag{A 4}$$

where

$$Re_q = \frac{Re\,q_\infty}{\alpha(b - c)}, \quad Re_b = \frac{Re(b - c)}{\alpha}. \tag{A 5}$$

When $b \gg |c|$, we have the condition $|Re_b| \gg |Re_q|$, and we can treat $|Re_q|^{-1}$ as a small expansion parameter. The lowest-order solution of (A 4) is then $\gamma^2 = \alpha^2$ or $\alpha^2 + \mathrm{i}\alpha Re(b - c)$, and the rapid-distortion effects appear at first order. In fact,

$$\gamma = \begin{cases} \gamma_1 = -\alpha\left[1 + \dfrac{q_\infty}{(b - c)^2}(\beta_1 + \beta_2 - \mathrm{i}\beta_3)\right], \\ \gamma_2 = -\alpha\sqrt{\mathrm{i}Re_b}\left[1 + \dfrac{q_\infty}{(b - c)^2}\dfrac{\beta_1 Re_b}{2}\right], \quad |Re_b| \gg 1. \end{cases} \tag{A 6}$$

Note, however, that the rapid-distortion effects appear non-perturbatively in γ_2 for sufficiently large values of $|Re_b|q_\infty$. The exact condition is $\beta_1 q_\infty Re_b/(b - c)^2 = O(1)$, which equates to

$$\alpha \lesssim \frac{\beta_1 q_\infty Re}{|b - c|}. \tag{A 7}$$

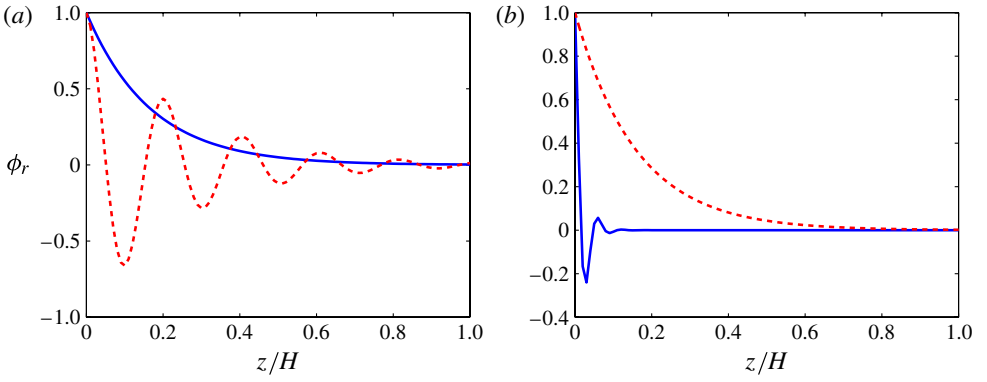

FIGURE 23. Far-field stream function in the toy model with typical parameter values $Re = 10\,000$, $c_r = 0.1$, $q_\infty = 10^{-3}$ and $\alpha = 2\pi$. Solid line, $\Re(\widetilde{\psi})$; broken line, $\Im(\widetilde{\psi})$. The coefficients β_1, β_2 and β_3 are taken from § 3. (*a*) $b = 0.1$; (*b*) $b = 0.3$. The oscillations are damped when the rapid-distortion domain is moved away from the interface.

Thus, the range of wavenumbers across which rapid distortion induces oscillations in the stream function is controlled by b. As $b \to \infty$, the rapid-distortion domain is pushed further and further away from the interface, and the oscillations appear in a narrower and narrower band of the spectrum. This analysis is confirmed by the stream function plots in figure 23, where we plot the rapid-distortion stream function for different b-values. There is a clear difference between the two cases shown: the oscillation is damped at higher b-values (figure 23*b*). Although our review of the experimental evidence has not evinced any support for these oscillations, they are similar to those obtained by Zaki & Saha (2009) in their study of the interaction between disturbances in the free stream and the boundary layer, wherein the continuous-spectrum Orr–Sommerfeld equation was used.

REFERENCES

ABRAMOWITZ, M. & STEGUN, I. A. 1965 *Handbook of Mathematical Functions*. Dover.

ABRAMS, J. & HANRATTY, T. J. 1985 Relaxation effects observed for turbulent flow over a wavy surface. *J. Fluid Mech.* **151**, 443–455.

ACHESON, D. J. 1990 *Elementary Fluid Dyanmics*. Oxford University Press.

BELCHER, S. E., HARRIS, J. A. & STREET, R. L. 1994 Linear dynamics of wind waves in coupled turbulent air–water flow. Part 1. Theory. *J. Fluid Mech.* **271**, 119–151.

BELCHER, S. E. & HUNT, J. C. R. 1993 Turbulent shear flow over slowly moving waves. *J. Fluid Mech.* **251**, 109–148.

BELCHER, S. E. & HUNT, J. C. R. 1998 Turbulent flow over hills and waves. *Annu. Rev. Fluid Mech.* **30**, 507–538.

BENJAMIN, T. B. 1959 Shearing flow over a wavy boundary. *J. Fluid Mech.* **6**, 161–205.

BIBERG, D. 2007 A mathematical model for two-phase stratified turbulent duct flow. *Multiphase Sci. Technol.* **19**, 1–48.

BOOMKAMP, P. A. M., BOERSMA, B. J., MIESEN, R. H. M. & V. BEIJNON, G. 1997 A Chebyshev collocation method for solving two-phase flow stability problems. *J. Comput. Phys* **132**, 191–200.

BOOMKAMP, P. A. M. & MIESEN, R. H. M. 1996 Classification of instabilities in parallel two-phase flow. *Intl J. Multiphase Flow* **22**, 67–88.

COHEN, J. E. & BELCHER, S. E. 1998 Turbulent shear flow over fast-moving waves. *J. Fluid Mech.* **386**, 345–371.

COHEN, L. S. & HANRATTY, T. J. 1965 Generation of waves in the concurrent flow of air and a liquid. *AIChE J.* **11**, 138–144.

CRAIK, A. D. D. 1966 Wind-generated waves in thin liquid films. *J. Fluid Mech.* **26**, 369–392.

DRAZIN, P. G. & REID, W. H. 1981 *Hydrodynamic Stability*. Cambridge University Press.

VAN DUIN, C. A. & JANSSEN, P. A. E. M. 1992 An analytic model of the generation of surface gravity waves by turbulent air flow. *J. Fluid Mech.* **236**, 197–215.

FULGOSI, M., LAKEHAL, D., BANERJEE, S. & DE ANGELIS, V. 2002 Direct numericical simulations of turbulence in a sheared air–water flow with a deformable interface. *J. Fluid Mech.* **482**, 319–345.

HANRATTY, T. J. 1983 Interfacial instabilities caused by air flow over a thin liquid layer. In *Waves on Fluid Interfaces*, pp. 221–259. Academic.

HEWITT, G. F. & HALL-TAYLOR, N. S. 1970 *Annular Two-Phase Flows*. Pergamon.

HRISTOV, T. S., MILLER, S. D. & FRIEHE, C. A. 2003 Dynamical coupling of wind and ocean waves through wave-induced air flow. *Nature* **422**, 55–58.

IERLEY, G. & MILES, J. 2001 On Townsend's rapid-distortion model of the turbulent-wind–wave problem. *J. Fluid Mech.* **435**, 175–189.

JANSSEN, P. A. E. M. 2004 *The Interaction of Ocean Waves and Wind*. Cambridge University Press.

KIHARA, N., HANAZAKI, H., MIZUYA, T. & UEDA, H. 2007 Relationship between airflow at the critical height and momentum transfer to the traveling waves. *Phys. Fluids* **19**, 015102.

KURU, W. C., SANGALLI, M., UPHOLD, D. D. & MCCREADY, M. J. 1995 Linear stability of stratified channel flow. *Intl J. Multiphase Flow* **21**, 733–753.

LAUNDER, B. E., REECE, G. J. & RODI, W. 1975 Progress in the development of a Reynolds-stress turbulence closure. *J. Fluid Mech.* **68**, 537–566.

LIN, M.-Y., MOENG, C.-H., TSAI, W.-T., SULLIVAN, P. P. & BELCHER, S. E. 2008 Direct numerical simulation of wind–wave generation processes. *J. Fluid Mech.* **616**, 1–30.

LOMBARDI, P., DE ANGELIS, V. & BANERJEE, S. 1995 Direct numerical simulation of near-interface turbulence in coupled gas–liquid flow. *Phys. Fluids* **8**, 1643–1665.

MASTENBROEK, C., MAKIN, V. K., GARAT, M. H. & GIOVANANGELI, J. P. 1996 Experimental evidence of the rapid distortion of turbulence in the air flow over water waves. *J. Fluid Mech.* **318**, 273–302.

MEIRINK, J. F. & MAKIN, V. K. 2000 Modelling low-Reynolds-number effects in the turbulent air flow over water waves. *J. Fluid Mech.* **415**, 155–174.

MIESEN, R. & BOERSMA, B. J. 1995 Hydrodynamic stability of a sheared liquid film. *J. Fluid Mech.* **301**, 175–202.

MILES, J. W. 1957 On the generation of surface waves by shear flows. *J. Fluid Mech.* **3**, 185–204.

MILES, J. W. 1959 On the generation of surface waves by shear flows. Part 2. *J. Fluid Mech.* **4**, 568–582.

MILES, J. W. 1962 On the generation of surface waves by shear flows. Part 4. *J. Fluid Mech.* **13**, 433–448.

Ó NÁRAIGH, L. & SPELT, P. D. M. 2010 Interfacial instability of turbulent two-phase stratified flow: pressure-driven flow and non-Newtonian layers. *J. Non-Newtonian Fluid Mech.* **165**, 489–508.

Ó NÁRAIGH, L., SPELT, P. D. M., MATAR, O. K. & ZAKI, T. A. 2011 Interfacial instability of turbulent two-phase stratified flow: pressure-driven flow and thin liquid films. *Intl J. Multiphase Flow* **37**, 812–830.

ÖZGEN, S., DEGREZ, G. & SARMA, G. S. R. 1998 Two-fluid boundary layer stability. *Phys. Fluids* **10**, 2746–2757.

PLANT, W. J. 1982 A relation between wind stress and wave slope. *J. Geophys. Res.* **C87**, 1961–1967.

POPE, S. B. 2000 *Turbulent Flows*. Cambridge University Press.

SULLIVAN, P. P., MCWILLIAMS, J. C. & MOENG, C.-H. 2000 Simulation of turbulent flow over idealized water waves. *J. Fluid Mech.* **404**, 47–85.

THORSNESS, C. B., MORRISROE, P. E. & HANRATTY, T. J. 1978 A comparison of linear theory with measurements of the variation of shear stress along a solid wave. *Chem. Engng. Sci.* **33**, 579–592.

TOWNSEND, A. A. 1972 Flow in a deep turbulent boundary layer over a surface distorted by water waves. *J. Fluid Mech.* **55**, 719–735.

TOWNSEND, A. A. 1980 The response of sheared turbulence to additional distortion. *J. Fluid Mech.* **81**, 171–191.

TSELUIKO, D. & KALLIADASIS, S. 2011 Nonlinear waves in counter-current gas–liquid film flow. *J. Fluid Mech.* **673**, 19–59.

VALLURI, P., Ó NÁRAIGH, L., DING, H. & SPELT, P. D. M. 2010 Linear and nonlinear spatio-temporal instability in laminar two-layer flows. *J. Fluid Mech.* **656**, 458–480.

YIANTSIOS, S. G. & HIGGINS, B. G. 1988 Linear stability of plane Poiseuile flow of two superposed fluids. *Phys. Fluids* **31**, 3225–3238.

YIH, C. S. 1967 Instability due to viscosity stratification. *J. Fluid Mech.* **27**, 337–352.

ZAKI, T. A. & SAHA, S. 2009 On shear sheltering and the structure of vortical modes in single and two-fluid boundary layers. *J. Fluid Mech.* **626**, 111–148.

ZEISEL, A., STIASSNIE, M. & AGNON, Y. 2007 Viscous effects on wave generation by strong winds. *J. Fluid Mech.* **597**, 343–369.

ZILKER, D. P., COOK, G. W. & HANRATTY, T. J. 1976 Influence of the amplitude of a solid wavy wall on a turbulent flow. Part 1. Non-separated flows. *J. Fluid Mech.* **82**, 29–51.